Small-scale variations of climate change in mountainous-forested terrain

A study from the H.J. Andrews Long Term Ecological Research site, Oregon, USA

Master's Thesis

Author: Kateřina Honzáková

Advisers: Prof. Dr. Christoph K. Thomas, Dr. Peter Hoffmann

Global Change Ecology

University of Bayreuth

8th August 2017

Abstract

The influence of topography on regional climate change remains a poorly understood phenomenon. In this thesis, long-term temperature records from the H.J. Andrews Experimental Forest (HJA), Oregon, USA and six stations from the Snotel network at a distance 20 - 50 km from the HJA were analyzed. Temperature patterns of the study area were investigated, with a focus on comparing valley and ridge stations. In particular, trends of the last day of frost, length of the vegetation period, temperature and the annual number of cyclonic, anti-cyclonic and zonal winds were explored. Additionally, the effect of homogenization of the temperature time series prior to analysis was considered. During the study period (1958 - 2011), the valley stations considered showed more consistent trends of an earlier last day of frost and warming daily minimum temperatures compared to stations at higher elevations. Changes in synoptic forcing towards more cyclonic activity and hence less cold air pooling in spring could serve as a reasonable explanation of these results. Data homogenization was found to considerably affect the temperature trends obtained. Further research and more data are needed.

Contents

Acknowledgements

I would like to thank my family and friends for their support and encouragement.

I would also like to thank my advisors, Dr. Peter Hoffmann from the Potsdam Institute for Climate Impact Research, especially for his help with the Python programming language and his support and encouragement and Prof. Dr. Christoph Thomas for sharing his knowledge, enthusiasm and for organizing our group visit to the European Geosciences Union Conference. Finally, I would like to thank BAYHOST for their financial support.

1 Introduction

1.1 Motivation

A mountainous terrain covers 20-25% of the Earth's surface, depending on which definition is used (Barry & Blanken, 2016) and mountain-based resources indirectly sustain most of the global population (Beniston, 2006). With climate change threatening global population as well as ecosystems, knowledge about responses of mountain climates on a regional scale is becoming crucial. For example, to predict streamflows, it is necessary to know where precipitation will fall as rain and where as snow, which could be predicted if one knows the temperature distribution (Minder et al. 2010). Accurate climate change predictions would enable us to better predict responses of ecosystems, e.g. an upward motion of species.

It is known that climate change has a high spatial variability (IPCC 2007, Daly *et al.*, 2010). However, climate models are mostly too crude to account for smaller scale features such as topography or to resolve sub-km scale air temperature distribution relevant to biota living in narrow mountain valleys (Holden *et al.*, 2011).

1.2 Objectives

In this study, long-term temperature records from the H.J. Andrews Experimental Forest (HJA), Oregon, USA and six stations from the Snotel network at a distance of 20 - 50 km from the HJA (Fig. 3.1 and 3.3) were analyzed. Temperature patterns were investigated with a focus on comparing valley and ridge stations' responses to climate change. Specifically, trends of the last day of frost, the length of the vegetation period and temperature trends were explored.

There are many factors affecting near surface temperature patterns (see Chapter 2). This thesis attempts to explain some of the temperature trends by investigating synoptic wind patterns (in particular the annual number of cyclonic, anti-cyclonic and zonal days) and wind speed and direction.

1.3 Hypothesis

The hypothesis was that the stations located at mountain ridges will show more pronounced warming trends compared to stations located in valleys. As suggested by e.g. Daly *et al.* (2010), valley stations are more decoupled from the free troposphere above compared to ridge stations due to a temperature inversion created when cold air pooling occurs. This could lead to a less prominent climate warming signal in valleys.

2 Theory

2.1 Factors affecting surface and near-surface temperature in a mountainous terrain

There are many factors affecting the surface and near-surface temperature. Wind facilitates thermal convection on and near the surface. Radiative heat transfer is governed by the radiation budget of solar (short-wave) and terrestrial (long-wave) radiation. Heat is transferred from and into soil layers by thermal conduction. Also phase changes play a role - latent heat is absorbed during ice melting and vaporization and released during condensation and freezing.

2.1.1 Wind and topography

In this thesis, 'wind' refers to motion of air. This could be at various scales and speeds. Topographic characteristics such as slope, aspect and exposure of surface to solar radiation and to winds affect local climates (Beniston, 2006; Smith, 2002; Geiger *et al.*, 1995). Topography is also influencing the airflow near the surface (Smith, 2002). Vice versa, temperature gradients cause pressure gradients, which drive winds. Here, two phenomena specific for mountainous regions are considered: cold air drainage and pooling.

Cold air drainage and pooling were described by Daly *et al.* (2010) and other studies, dating back to 1914 (Marvin, 1914). On a clear day, when the radiation balance is negative[1] (i.e. the surface is warming, $\sim$ day-time), the air near the surface is warming faster than the air at the same elevation further away from the surface. The warmer air will rise and, on a slope, an up-slope flow forms. However, when the radiation balance is positive ($\sim$ night-time), the air near the surface is cooling faster and when there is a small amount of vertical mixing (i.e. weak winds) a down-slope flow forms, referred to as cold air drainage. This diurnal pattern of up- and down-slope flow is present in all mountain regions (Beniston, 2006; Lundquist *et al.*, 2008). Similarly, in a valley with an altitudinal gradient, there are up-valley flows during

[1] Here the sign convention as in e.g. Foken & Nappo (2008), defining fluxes away from the surface as positive and those directed towards the earth's surface as negative, is used.

the day and down-valley flows during the night. These winds are the strongest when skies are clear and the synoptic winds are weak, since diurnal mountain circulation patterns can be disturbed by interference with synoptic winds (Whiteman, 2000).

As the air drains down the slope, it can form cold air pools in valleys, referred to as cold air pooling, which causes local temperature inversions. When this occurs, the warmest air of a valley is found in a thermal belt at the top on the inversion, midway up the slope (Whiteman, 2000). Due to a lack of vertical mixing, a cold air pool within a valley is effectively decoupled from the free troposphere above (Daly *et al.*, 2010). The temperature difference between the valley bottom and an adjacent hill slope can be 6 K or even more (Bootsma, 1976; Whiteman, 2000). Actual drainage flows are often intermittent (Mahrt *et al.*, 2010).

Although cold air drainage and pooling are widespread even on weak slopes (Mahrt *et al.*, 2010), their responses to climate change are largely unknown. General circulation models (GCMs) are too crude ($\sim$ 50 km resolution) to account for topography and hence not useful to simulate future cold air drainage and pooling. Moreover, due to the decoupling from the free atmosphere, cold air pools might respond differently to climate change than what would be typical for a given region (Daly *et al.*, 2010).

Valley geometry needs to be considered as well. Cold air drainage on a slope that gets steeper with increasing elevation creates a horizontal pressure gradient that drives nocturnal down-valley winds. On the other hand, when the steepness decreases with elevation there are stable conditions and cold air pooling. The situation is also different for channel-like valleys with a preferred wind direction (along the channel) and cone-like valleys (no preferred wind direction) as the former will likely experience stronger winds and hence more mixing (Lundquist *et al.*, 2008).

Synoptic winds also need to be taken into account. Daly *et al.* (2010) found out that anti-cyclonic flows with a low flow strength lead to more pronounced cold air pooling and hence stronger temperature inversions, whereas cyclonic flows with a high flow strength showed the steepest temperature drop with altitude (Fig. 3.8). Therefore, regions with a predicted increase in the number of cyclonic days are likely to experience less cold air pooling and valleys might experience greater degree of warming than hill slopes and crests.

2.1.2 Other factors

There are other factors affecting the near-surface temperature. For example, vegetation cover affects the amount of solar radiation reaching the surface and also airflows in its proximity (Smith, 2002). Clouds affect the radiation budget by absorbing part of the solar radiation and also emitting radiation themselves. Surface emissivity, the albedo and thermal conductivity also play a role.

In the case of the HJA, another factor needs to be considered. There is a water body (Blue River Lake) at the mouth of the valley (Fig. 3.1b). In general, water surfaces take longer to change temperature than land surfaces due to their larger heat capacity (Aguado, 2016). Therefore, the lake has a warming effect on the surrounding area during the periods of positive radiation balance ($\sim$ night time) and a cooling affect when the radiation balance is negative ($\sim$ day time). Hence, two competing flows in the HJA valley might occur during the night-time: a down-valley flow caused by cold air drainage and up-valley flow cased by the lake being warmer than the surrounding land surface.

2.2 Predictions

2.2.1 Temperatures

Globally, on average, both the daily minimum temperature (T_{min}) and the daily maximum temperature (T_{max}) have shown increasing trends since 1950, with most of the increase since 1980 (Vose *et al.*, 2005; Stocker *et al.*, 2013). A number of studies in the US found that T_{min} records have been showing more pronounced warming trends than T_{max} records (Easterling, 2002). Greenland (1994) observed an increase in the minimum, maximum and mean temperatures in the HJA in the period 1973 - 1991. The greatest increases occurred in spring months (March-May). Jones (2010) studied monthly means of T_{min} and T_{max} for some of the HJA stations and found that most of the stations experienced warming trends for the majority of months of the year.

The last day of frost (LDOF) marks the beginning of the vegetation period. The LDOF was defined as the last day when $T_{min} < 0°C$, also referred to as the last-spring freeze (Easterling, 2002) and followed by a frost-free season. In latitudes corresponding to the study region, the LDOF usually occurs in spring, however, at high elevations it is shifted to later dates and it is non-existent in permanently frozen areas. According to Kunkel *et al.* (2004), the LDOF has been occurring earlier since 1980 in the US on average.

The length of the vegetation period (LOVP), also referred to as the length of the frost-free season (Kunkel *et al.*, 2004), is an important parameter for organisms. Here it was defined as the period where $T_{min} \geq 0°C$. Since 1980, the LOVP has been increasing the in US on average, and the increase has been greater in the western US (Kunkel *et al.*, 2004).

2.2.2 Synoptic patterns

According to the IPCC AR4 (Jones *et al.*, 2007) considering large scale climate models, the annual precipitation will increase and the surface pressure is projected to decrease in the area including the study region. Since anti-cyclonic days are typically dry with high surface pressure (Daly *et al.*, 2010), these changes would indicate a decrease in the annual number of anti-cyclonic days in this area. However, according to the Jones *et al.* (2007), these projections are still quite uncertain.

3 Materials and Methods

3.1 Study site

The data was taken from the H.J. Andrews Experimental Forest (HJA), Oregon, US (Figure 3.1) and six stations from the Snotel network at a distance 20 - 50 km from the HJA.

The HJA is a part of the US Long Term Ecological Research Network (LTER) and it has operated since 1948. It is located on the western slope of the Cascade Mountains in Oregon with elevation ranging from 412 m to 1627 m. It attracts scientists from a variety of disciplines, and provides a unique opportunity to study mountain climate due to its dense network of stations, long-term records and a distinct mountainous topography. Regarding the vegetation, there are conifer-dominated forests, some of which have been growing without human management for several centuries (Daly *et al.*, 2010; Smith, 2002; HJA Website, 2017*a*). The results could potentially be generalized to other areas since the HJA's climate is representative of mountainous areas of the Pacific Northwest (Smith, 2002; Daly *et al.*, 2010).

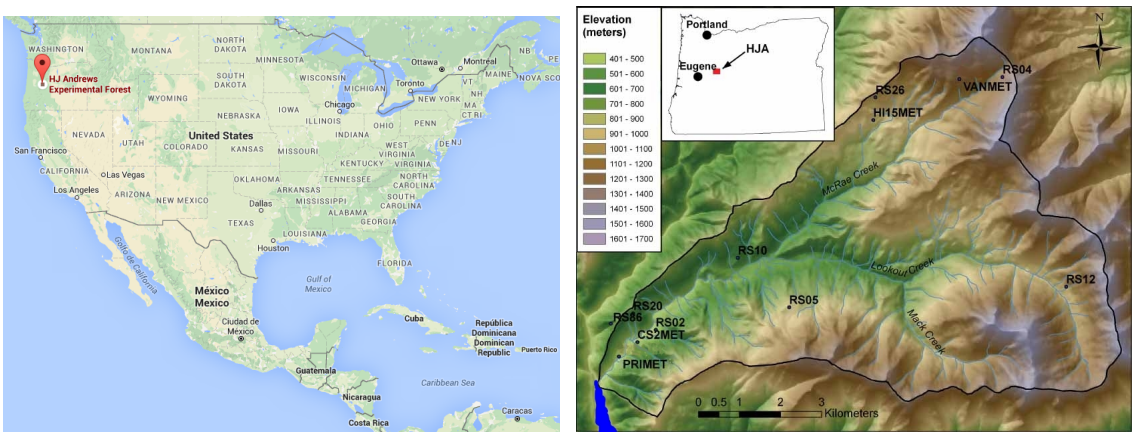

(a) (b)

Figure 3.1: Location (a) and topographic relief map (b) of the HJA. Sources: Google Maps and Daly *et al.* (2010), respectively.

The HJA has a Mediterranean climate with wet winters and dry summers and annual precipitation between 2227 mm/year at 430 m above the sea level (asl) and 2712

mm/year at 1294 m asl (Daly *et al.*, 2010). It has a pronounced topography with steep slopes and narrow valleys highly susceptible to cold air drainage and pooling, and night-time temperature inversions are common both in summer and winter (Daly *et al.*, 2010; Smith, 2002).

3.2 Data and variables

Troughout this text, abbreviated forms of station names are used, e.g. PRIMET instead of *Primary Meteorological Station*. Stations within the HJA have abbreviations consisting of capital letters and numbers only, whereas Snotel stations are referred to by combinations of upper- and lower- case letters. There are five 'benchmark' stations within the HJA: PRIMET, VANMET, CENMET, UPLMET and HI15MET. For those, measurements at two heights above the ground were included: 150 cm and 450 cm. For example, to refer to PRIMET measurements at height 150 cm, abbreviation PRIMET150 is used and analogously for the height 450 and the other benchmark stations. Please see Table A.1 in the Appendix for full names of the stations and information about their latitude, longitude, elevation, slope and aspect.

3.2.1 HJA

For the HJA, the data used came from six meteorological stations: PRIMET, CS2MET, VANMET, CENMET, UPLMET and HI15MET and 17 reference stands (RS) in forests: RS 1 - 5, 7, 10, 12, 13, 15 - 17, 20, 24, 26, 86 and 89 (Fig. 3.2). Stations were divided into 'valley' and 'ridge' stations, as described in section 3.3.1. For further information about the HJA measurement sites (such as sensors used, canopy, surface and general site characteristics) see the HJA Website (2017*a*) and Smith (2002), Table F.1., pages 189 - 211.

3.2.2 Snotel

Snotel (short for SNOw TELemetry) is a network of stations primarily aimed at snow monitoring operated by the United States Department of Agriculture Natural Resources Conservation Service (USDA NRCS). For our purpose, daily T_{min} and T_{max} data were used. More information about Snotel can be found on their website (USDA NRCS, 2016*b*). The stations considered were ThreeCreeksMeadow, McKenzie, RoaringRiver, HoggPass, SantiamJunction and JumpOffJoe, at a distance 20-50 km from the HJA (Fig. 3.3).

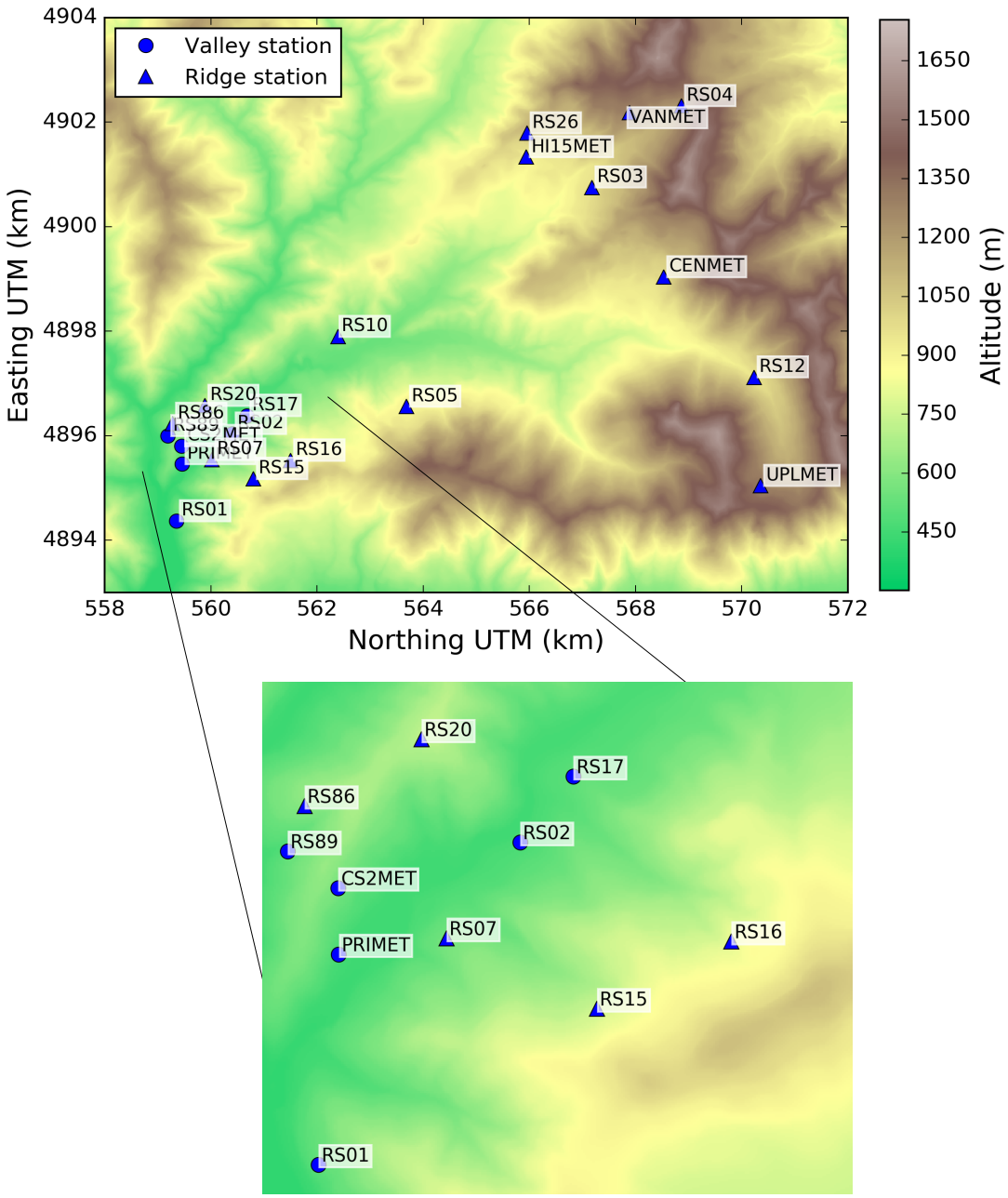

Figure 3.2: Map showing names and positions of the HJA stations.

The variables considered were T_{min} and T_{max} air temperature with daily resolution from 1958 until 2011. The data were provided by C.K. Thomas (2011). During the time period studied (1958 - 2011), the methods and devices used to measure and record T_{min} and T_{max} were evolving. Detailed information about measurement methods and devices for the HJA stations can be accessed on the HJA website, Measurements Information section (2017). For the Snotel network, this information is

available on the Snotel website (2017) under 'Station Information' (station, variable and time-period of interest must be specified first).

Additionally, horizontal wind direction and speed from the benchmark stations were considered. The start of the measurement period was between 1992 and 1996 (depending on the station) and the end date was set to 31. 12. 2011 to correspond to T_{min} and T_{min} data. A propeller anemometer at height 5 to 12 m was used to obtain the wind data, available through online application GLITCH (General Linear Integrator for Time CHanging, 2016). More information about the wind data can be found in the section 3.9.

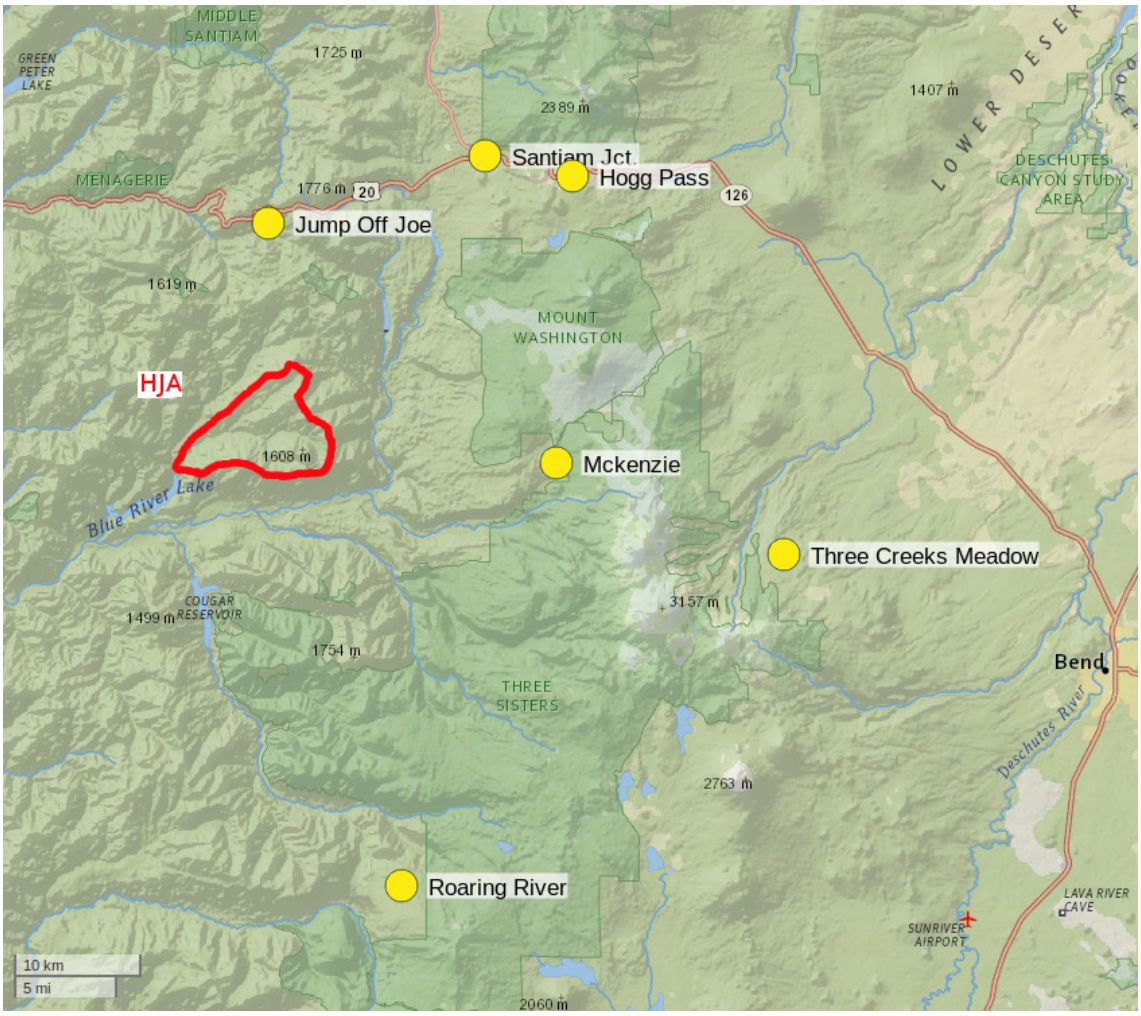

Figure 3.3: Map showing the positions of the Snotel stations and the HJA. It was created using the 3.0 Beta release of the National Water and Climate Center's Interactive Map (USDA NRCS, 2016*a*).

3.3 Data quality and homogenization

Long term datasets are prone to inhomogeneities caused by, for example, a change of devices, station location, or surrounding vegetation (Peterson & Easterling, 1994). The first step in our work was creating a homogenized dataset. Plausibility tests, despiking and initial quality control tests were performed. The standard Normal Homogeneity Test (SNHT) (Alexandersson, 1986; Alexandersson & Moberg, 1997) was used to detect breaks and shifts in the time series of the variables considered. A composite climate reference time series based on the Global Historic Climate Network was created and, together with cross-referencing against station records, was used to correct non-homogeneities in the data. The quality control and homogenization procedure was developed in Matlab (The MathWorks, Inc., 2017) by C. K. Thomas (2011) and can be seen in Fig. 3.4. The homogenization is an iterative process - it finds and corrects the largest break (shift) in the time series input and then it proceeds iteratively as long as there are breaks above a certain threshold (Fig. 3.5, bottom).

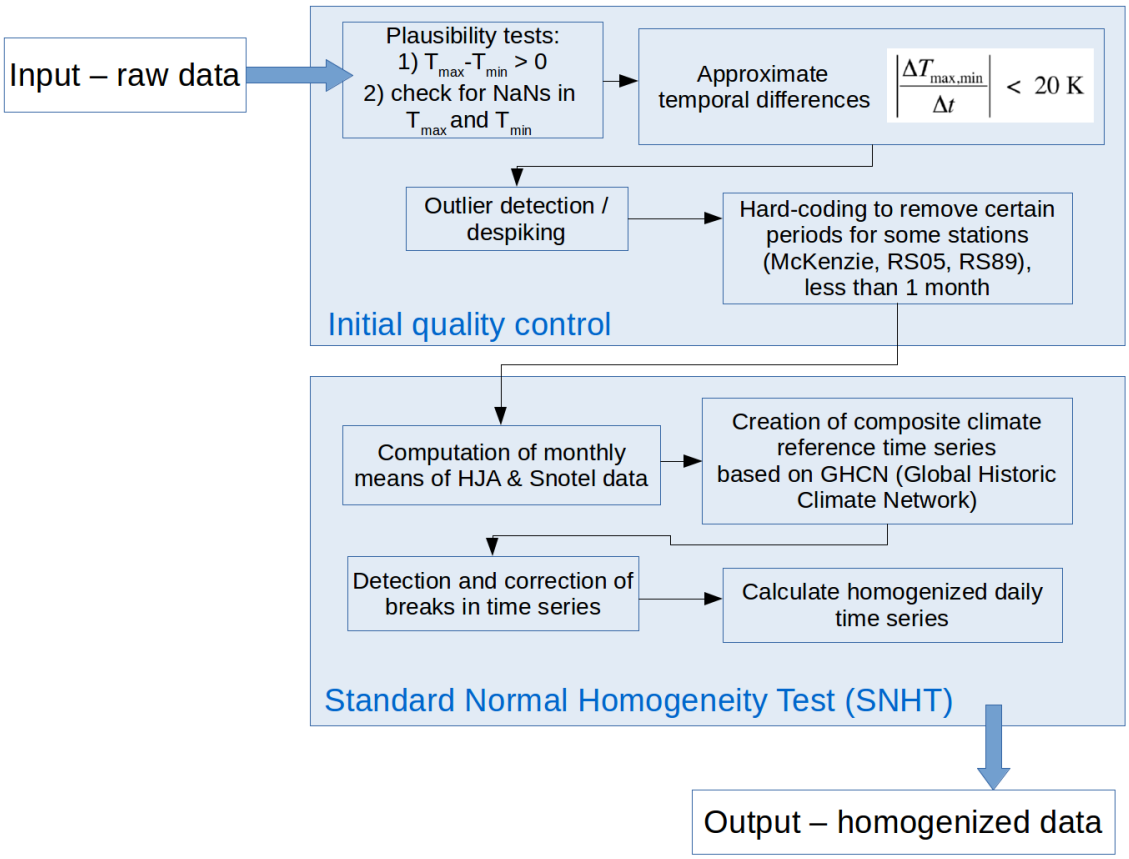

Figure 3.4: Data quality control and homogenization procedure developed by C. K. Thomas (2011).

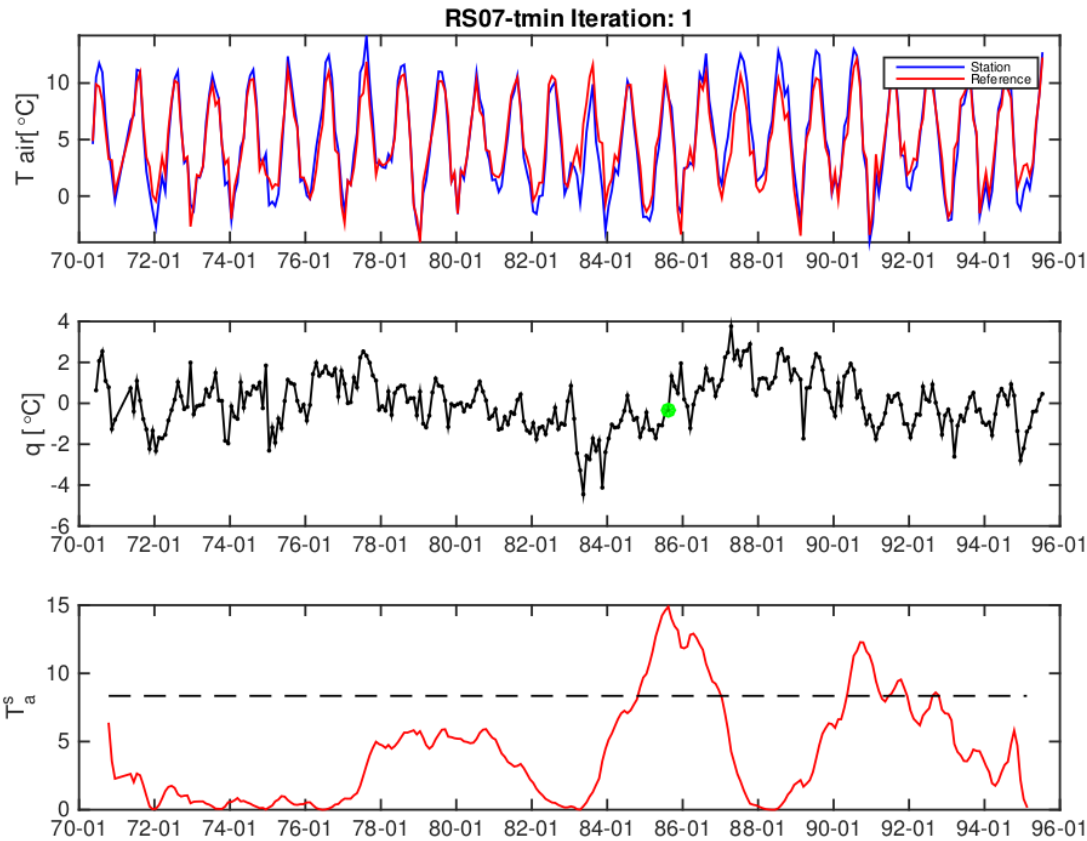

Figure 3.5: Example of the homogenization procedure for T_{min} at RS07. From top to bottom: 1. the time series recorded at RS07 (in blue) and a reference time series (red), 2. the time series of differences between recorded T_{min} and the reference series (as in 1.) showing a detected shift, 3. the result of the SHNT and a selected threshold for shifts. Shifts smaller than this threshold were not addressed.

3.3.1 Datasets

To correct for breaks and shifts in the T_{min} and T_{max} time series, a homogenized dataset was created as described above. However, some of the shifts could be a true temperature shifts and might not be caused by a change in devices or measurement methods in general. Most shifts were a part of several bigger clusters, close together in time and magnitude, but there were also outliers. These outlying shifts were not accepted in the 'partially-homogenized' dataset. To determine the effect that data homogenization has on the results, three datasets were analyzed (Table 3.1).

The stations were divided into two groups, according to their relative elevation as estimated from Lidar measurements:

1. Valley stations, here defined as the stations located less than 100 m above the valley bottom, i.e. below 530 asl.

2. Ridge stations - all the other stations.

According to the criteria above, there are five valley stations: PRIMET, RS02, CS2MET, RS01 and RS89. They are all located in the same valley within the HJA.

Table 3.1: Three datasets used.

Dataset	**Description**
Raw	Data as obtained from the stations.
Homogenized	Created from the raw dataset as shown in the flowchart in Fig. 3.4.
Partially-homogenized	Only shifts occurring in clusters were considered valid, outliers were not accepted.

3.4 Software

Apart from the data homogenization, which was done in Matlab (The MathWorks, Inc., 2017), the analysis was performed in Python (Python Software Foundation, 2017), utilizing its many packages, notably `scipy`. Spyder - Scientific Python Development Environment (2017) was used. Typesetting of this thesis was performed in Texmaker (Brachet, 2014), running pdfTeX (Thanh, 2015).

3.5 Last day of frost (LDOF)

It was assumed than the LDOF occurs within the first 200 days of each year. Starting at day of the year (DOY) 1 (i.e. January 1st), each DOY up to DOY 200 was checked and the last DOY with $T_{min} < 0°C$ was recorded; if there was a gap (NaN) between the last DOY with temperature below 0°C and DOY 200, the LDOF was set to NaN.

Afterwards, a trend in the LDOF for each station was calculated using a least squares linear fit. To quantify the significance of the trends (by means of their p-values), the Mann-Kendall test was performed. It is a non-parametric statistical test, described e.g. in Yue *et al.* (2002). A map utilizing the Universal Transverse Mercator (UTM) coordinate system and showing the stations within the HJA together with their LDOF trends was created (Fig. 4.1). At high elevations, frost can occur at any time of the year, therefore the LDOF is not meaningful there.

3.6 Length of the vegetation period (LOVP)

The LOVP was defined as the number of consecutive days where $T_{min} \geqq 0°C$. To calculate it, the LDOF and the first day of frost (FDOF, also referred to as the first autumn freeze) needs to be determined. The LDOF was calculated as described in the previous section. To calculate the FDOF, it was assumed that it occurs annually between the LDOF and the DOY 365. Starting at the LDOF, days were consecutively checked until the first DOY with a temperature below 0°C was found, this day was then recorded as the FDOF of the year considered. If a gap (NaN) was encountered before finding a DOY with a temperature below 0°C, the FDOF was set to NaN. Whenever the LDOF or the FDOF for a particular year was NaN, the LOVP was set to NaN.

Otherwise,

$$\text{LOVP} = \text{FDOF - LDOF}. \tag{3.1}$$

Afterwards, trends in the LOVP were calculated using a least squares linear fit and their p-values were determined.

3.7 T_{min} and T_{max} trends

For each DOY (ranging from 1 to 365) and each station, a least squares linear fit was used to calculate trends in T_{min} and T_{max} for this DOY using all available years (Fig. 3.6). Afterwards, a probability density function (PDF) of the DOY trends was constructed using least-squares regression (LSR). The maximum of the LSR PDF is a measure which can be used to quantify a 'net' temperature trend. The distribution of DOY trends differed for each station and was also affected by the dataset used, however, in most cases, the DOY trends had approximately Gaussian distributions.

'Net' trends of T_{min} and T_{max} were calculated as described above for all stations and datasets and a comparison between ridge and valley stations as well as among different datasets was made (Fig. 4.4, Tables 4.3 and 4.4). Additionally, means and standard deviations of all 365 DOY LSR trends were calculated.

Apart from the LSR, the Theil-Sen (TS) method was used to get a trend estimate that is less sensitive to outliers. Analogously to the LSR, for all the stations and datasets, the mean, standard deviation and PDF of corresponding DOY trends were calculated. For both of the LSR and TS methods, all trends were considered, regardless of their p-values. Fig. 4.5 shows an example for CS2MET and full results can be found in Tables A.4 - A.6 in the Appendix.

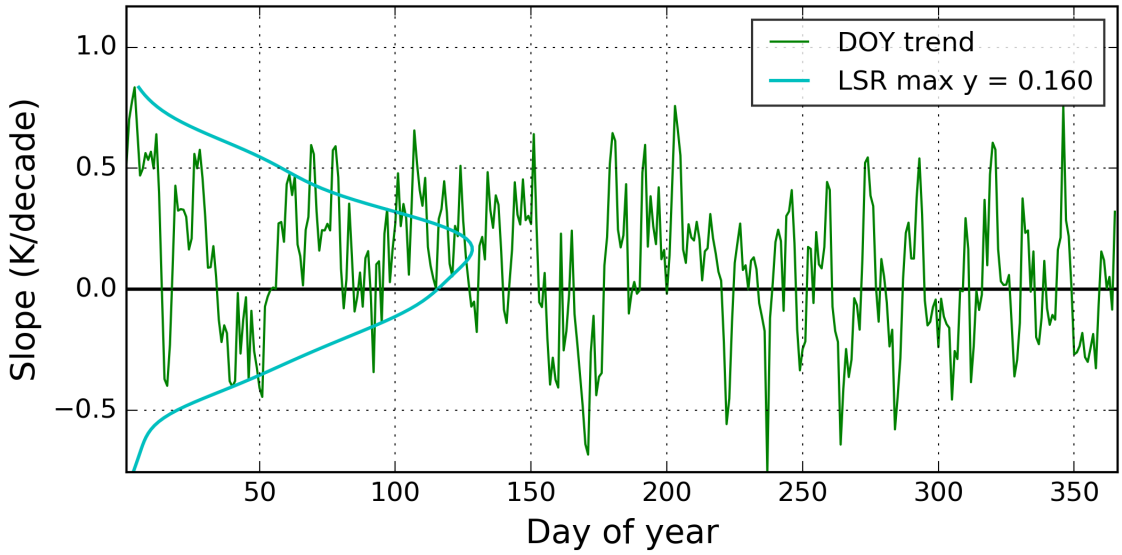

Figure 3.6: DOY trends for T_{min} at CS2MET (in green). A probability density function (PDF) of those trends was constructed using least-squares regression (in cyan). Its maximum corresponds to a warming trend of 0.16 K per decade.

3.8 Synoptic patterns

The change in synoptic patterns during the study period was examined. For each day, the mean lapse rate was taken to be the slope of elevation versus T_{min} plot (least squares linear fit); for example, see Fig. 3.7. Both the HJA and Snotel sites were considered and it was assumed that for each day the synoptic pattern is the same across our study area. This seems to be plausible since the extent of our study area (<100 km) is small compared to the synoptic scale (order of 1000 km).

To classify each date, the result obtained by Daly *et al.* (2010), Fig. 3.8, was used and three cases according to the lapse rate were considered:

1. lapse rate < -2.8 (K/km) ⇒ cyclonic day
2. 0 ≥ lapse rate ≥ -2.8 (K/km) ⇒ zonal day
3. lapse rate > 0 (K/km) ⇒ anti-cyclonic day

However, as apparent from Fig. 3.8, the border distinguishing zonal and cyclonic days is not clear cut. In the example of Fig. 3.7a, the lapse rate was approximately -3.6 K/km and according to Daly *et al.* (2010) this day would be classified as cyclonic (Fig. 3.8). The p-value of the fit was in this case approximately 0.013.

However, on another date, the situation might be different. There might not be enough stations available and/or the linear fit used to determine the lapse rate might

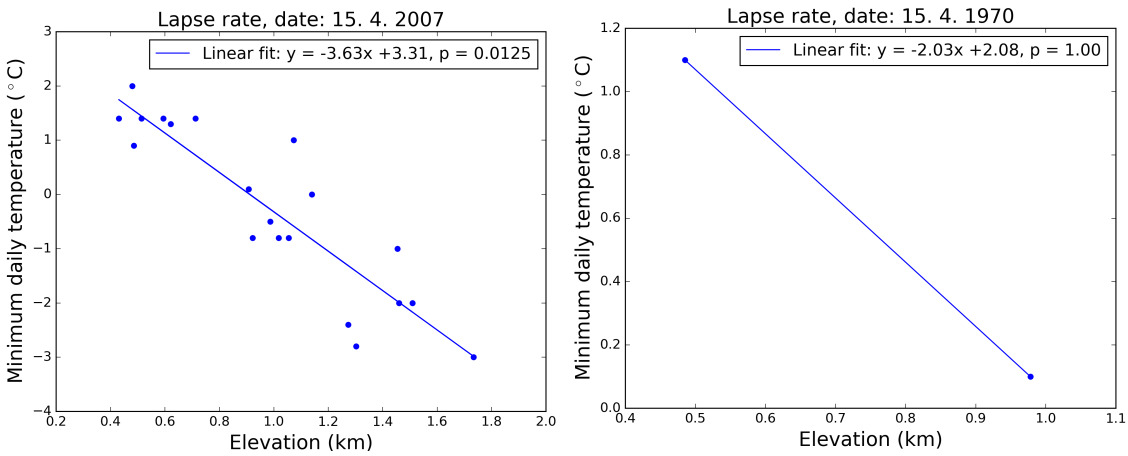

(a) (b)

Figure 3.7: Lapse rate determination, two examples. Each point represents one station.

have a large p-value (e.g. Fig. 3.7b). To address this, three different variants of conditions were employed:

(a) $n_s \geq 3$ and $p_c \leq 0.05$

(b) $n_s \geq 2$ and $p_c \leq 0.1$

(c) $n_s \geq 2$ and $p_c \leq 0.8$

where n_s is the number of stations available on the particular date and p_c is the maximum accepted p-value. In the case of $n_s < 2$, the lapse rate was not determined. (a) has the strictest criteria on the n_s and p_c, which leads to a more accurate synoptic pattern classification, however, most of the dates in our date range (1958 - 2011) did not meet this criteria. (b) and (c) have less strict criteria and hence are applicable to a greater number of dates, but are more prone to a misclassification of synoptic patterns.

Afterwards, for all variants of conditions, each day was classified as cyclonic, anti-cyclonic, zonal or NaN (if not enough data were available to classify it). Fig. 4.6 shows the results for the homogenized dataset. To be able to compare years with a differing number of NaNs (gaps), the numbers of cyclonic, anti-cyclonic and zonal days obtained were multiplied by a constant (i.e. scaled by the same factor) such that they would add up to 365 days for each year. Afterwards, trends in annual number of cyclonic, anti-cyclonic and zonal days were calculated. Fig. 4.7 shows the results for the raw dataset.

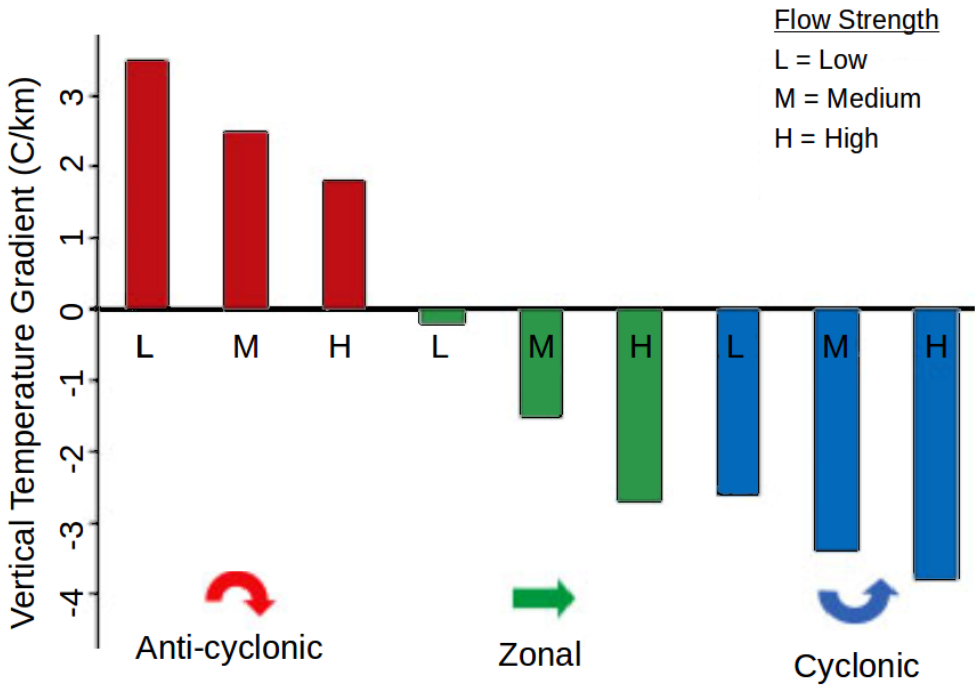

Figure 3.8: Definition of cyclonic, anti-cyclonic and zonal days according to the mean lapse rate. Source: Daly *et al.* (2010).

3.9 Wind speed and direction

This data was only available for the benchmark stations (CENMET, H15MET, PRIMET, UPLMET and VANMET). Mean hourly wind speed and direction data were downloaded from the HJA website. Regarding the data collection, the wind speed and direction were sampled every 15 seconds by a RM Young Model 05103 Wind Monitor with a detection limit of 1 m/s. It was mounted to a tower at the height of 10 m for CENMET, PRIMET and UPLMET and 5 m for H15MET. For VANMET, the height was changed on 27. 8. 1996 from 6 m to 10 m. Campbell Scientific datalogger was used in all cases (HJA Website, 2017*b*).

For each value of the wind direction or speed, there was a flag assigned indicating its reliability. Relevant to our case were flags 'A' - *Accepted value has passed all QC tests applied as represented by the quality level* and 'B' - *Wind magnitude measurement is below the instrument detection limit of 1 m/s.* A full list of flags can be accessed on the HJA website (HJA Website, 2017*b*). Two cases were considered:

1. Only 'A' flag was accepted for both wind speed and direction.
2. Only 'A' and 'B' flags were accepted for both wind speed and direction.

Since cold air pooling occurs at night, mean night-time wind direction was considered.

It was calculated as the vectorial mean of available wind velocities for each night, where the night-time was defined as 19-06 h. In the case of PRIMET, the only benchmark valley station, further analysis was performed. The results were sorted according to their direction: up-valley (NE, 0-90°) and down-valley (SW, 180-270°). To investigate the effect of night-time wind direction on T_{min}, the mean night-time direction was plotted against T_{min} perturbation, here defined as the difference from monthly mean (hence independent of season). Mean T_{min} and its standard deviation for both SW and NE directions were calculated.

4 Results

4.1 Last day of frost (LDOF)

The valley stations experienced earlier last day of frost (LDOF) trends during our study period for all three datasets, with only one exception (RS89 showed a later LDOF trend, but only when the partially-homogenized dataset was considered), whereas the ridge stations showed an inconsistent pattern (Fig. 4.1, Table A.2 in the Appendix).

The valley stations had negative median and mean values of the LDOF trends for all three datasets (indicating earlier LDOF), while the ridge stations had positive mean values and both positive and negative median values, depending on which dataset was used (Table 4.1). Overall, the majority of the stations showed an earlier LDOF trend and the trends differed depending on whether the raw, homogenized, or partially-homogenized dataset was used. Table 4.1 summarizes the LDOF trends, listing the median, mean, standard deviation, maximum and minimum trend values obtained. LDOF trends together with their p-values for all stations and all three datasets can be found in Table A.2. Most trends had p-values > 0.05.

(a)

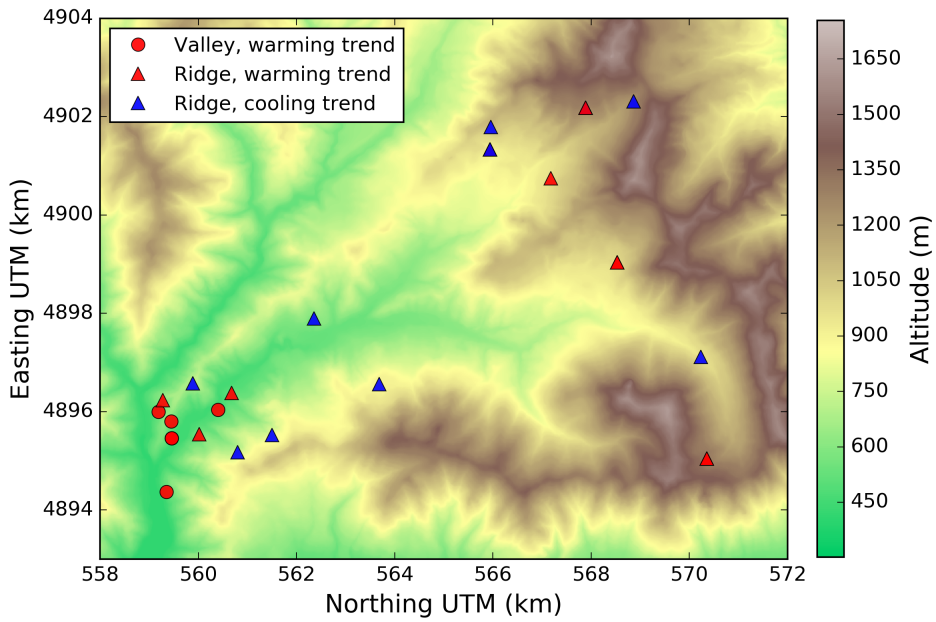

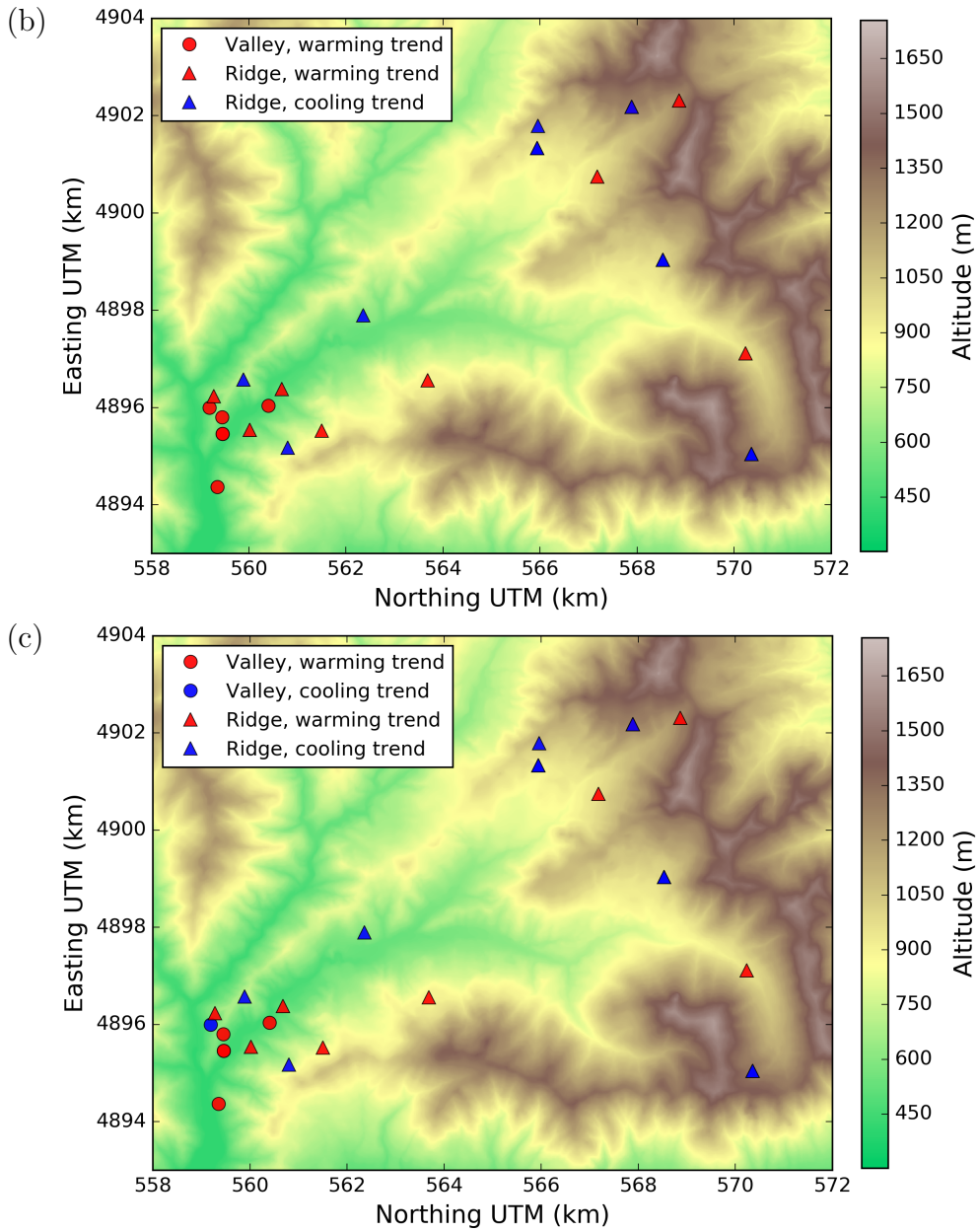

Figure 4.1: Trends of last day of frost (LDOF) for the HJA stations for (a) raw data, (b) homogenized data and (c) partially-homogenized data displayed on a topographic map of the HJA. The red-colored markers indicate earlier LDOF (i.e. 'warming') trends, whereas the blue ones indicate later LDOF ('cooling') trends. The valley and ridge stations are marked by circles and triangles, respectively. A Universal Transverse Mercator (UTM) coordinate system is used. The Snotel stations are not included in the picture.

Table 4.1: The median, mean, standard deviation, maximum and minimum values of the LDOF trends for all three datasets. Numbers are in days/year and rounded to two decimal places. Negative numbers indicate an earlier LDOF, whereas positive ones a later LDOF.

	Median	**Mean**	**St. dev.**	**Maximum**	**Minimum**
Valley stations					
Raw	-0.75	-0.81	0.27	-0.53	-1.33
Homogenized	-0.15	-0.17	0.17	-0.01	-0.40
Partially-homogenized	-0.38	-0.33	0.60	0.70	-0.97
Ridge stations					
Raw	0.16	0.24	0.90	2.94	-0.98
Homogenized	-0.01	0.26	0.94	2.94	-1.04
Partially-homogenized	-0.05	0.12	0.98	2.94	-1.33
All stations					
Raw	-0.05	0.06	0.91	2.94	-1.33
Homogenized	-0.02	0.19	0.87	2.94	-1.04
Partially-homogenized	-0.14	0.04	0.93	2.94	-1.33

4.2 Length of the vegetation period (LOVP)

For all three datasets, there seems to be no distinct patterns in the LOVP for the valley and ridge stations (Fig. 4.3, table 4.2). As mentioned in the Materials and Methods section, for the benchmark stations there are two measurement heights - 150 cm and 450 cm and the trends for these two hights may differ (this is indicated in Fig. 4.3 by purple markers). For UPLMET and CENMET, the LOVP trends differed for the two heights for all three datasets. For PRIMET, increasing LOVP trends were observed except for the homogenized dataset at measurement height 150 cm.

The LOVP trends' magnitudes are summarized in Table 4.2, which lists the minimum, mean, median and maximum trend values obtained. One can see that the dataset used had an impact on the results; in some cases using a different dataset resulted in a different sign of the LOVP trend. Table A.3 in the Appendix lists the LOVP trends together with their p-values for all stations and all three datasets. Most trends had p-values > 0.05.

The LOVP is more sensitive to the accuracy of, and the gaps, in the data, as both the LDOF in spring and the first day of frost (FDOF) in autumn need to be determined. For some of the stations (e.g. UPLMET, Fig. 4.2b, or VANMET150), gaps in the temperature data led to few LOVP data points available, which might have caused unreliable trend outcomes.

(a)

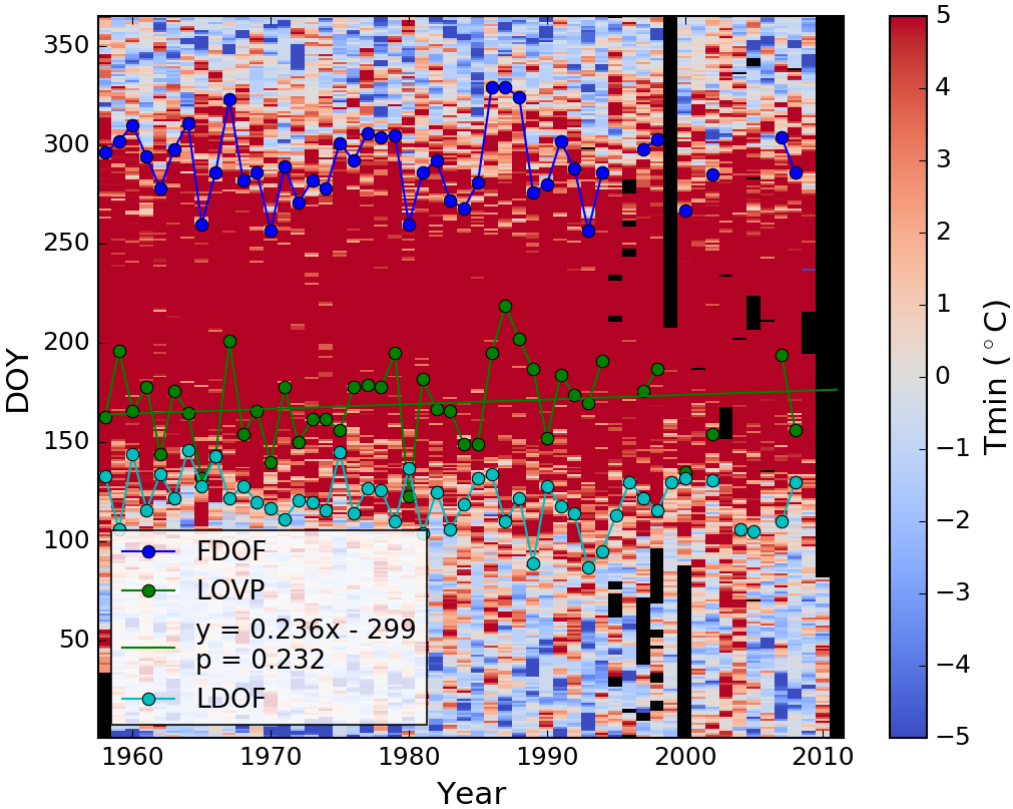
FDOF
LOVP
y = 0.236x - 299
p = 0.232
LDOF
DOY
Year
Tmin (°C)

(b)

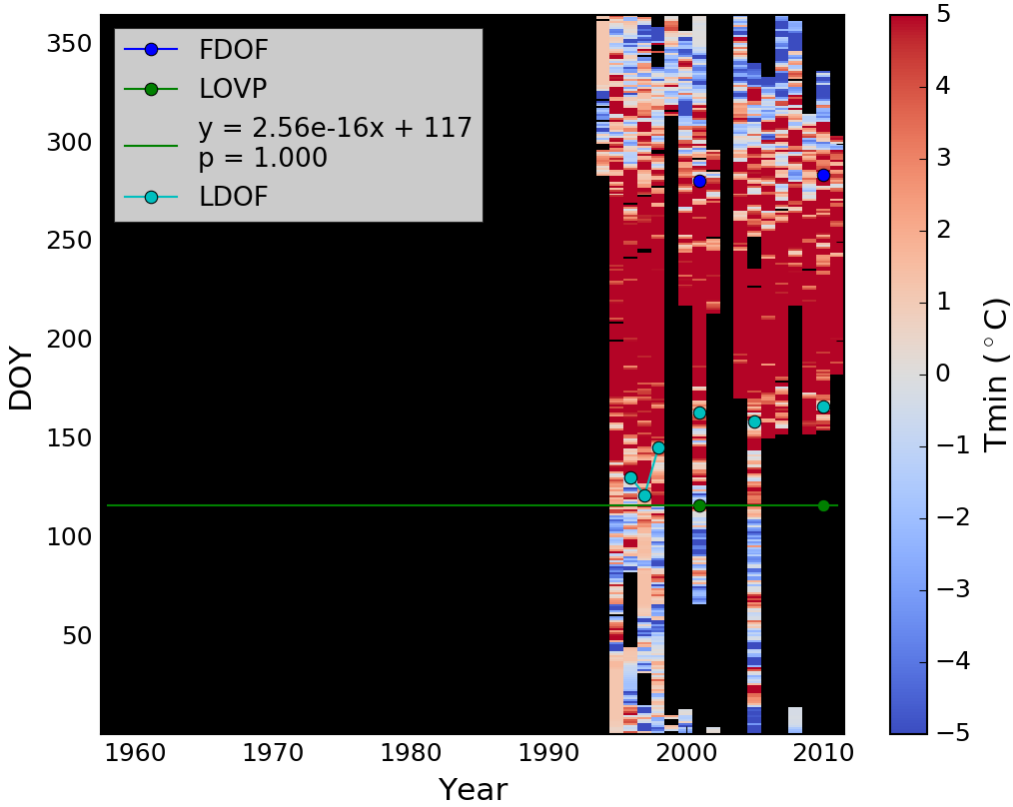
FDOF
LOVP
y = 2.56e-16x + 117
p = 1.000
LDOF
DOY
Year
Tmin (°C)

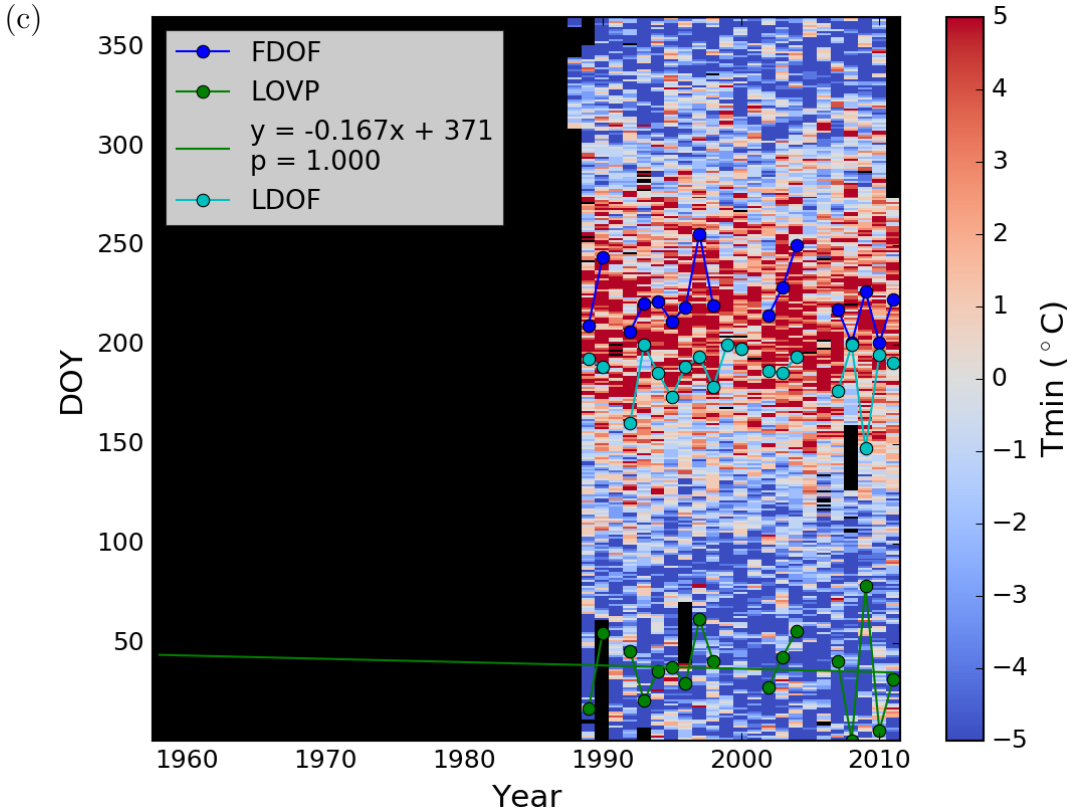

Figure 4.2: Hovmöller plots showing the first day of frost (FDOF, in blue), the last day of frost (LDOF, in cyan), the length of the vegetation period and its trend (both in green) using the homogenized dataset at (a) CS2MET (valley station, longest continuous record at the HJA), (b) UPLMET150 (ridge station) and (c) McKenzie (ridge, Snotel station). Black fields indicate no available data.

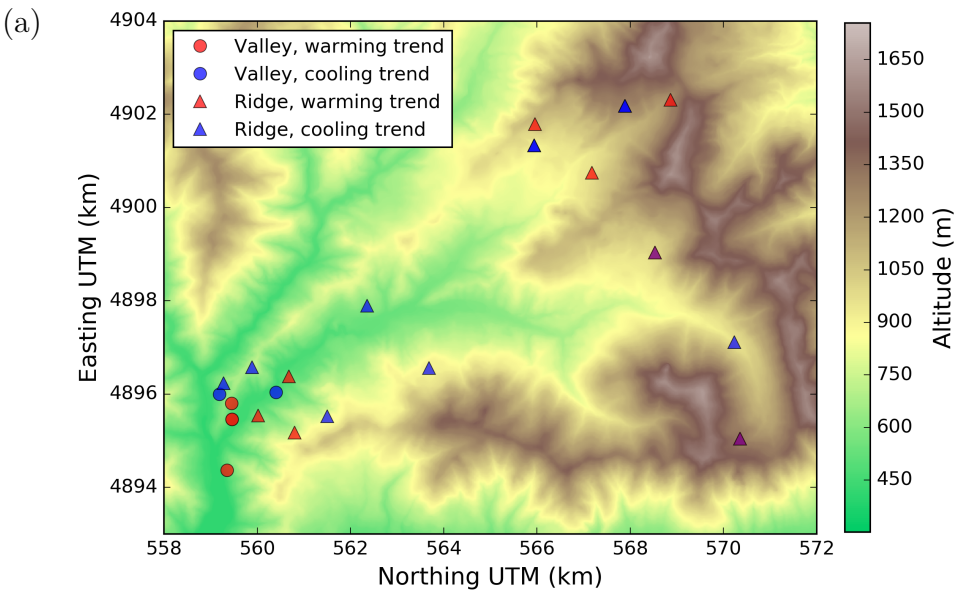

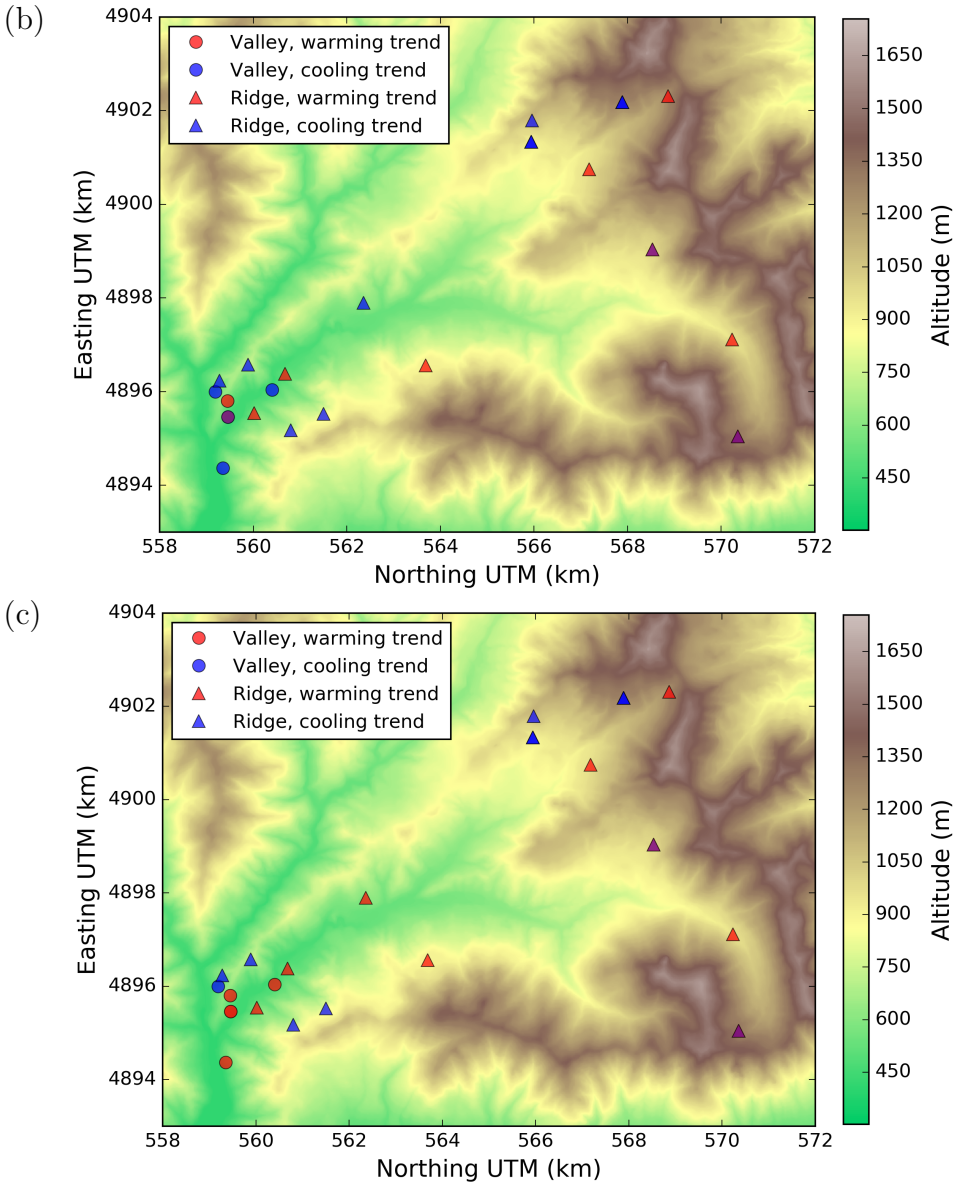

Figure 4.3: Trends of the LOVP for the HJA stations for (a) raw data, (b) homogenized data and (c) partially-homogenized data displayed on a topographic map of the HJA. The red-colored markers indicate increasing LOVP ('warming') trends, whereas the blue ones indicate decreasing LOVP ('cooling') trends. At stations with two measurement heights (150 and 450 cm) with opposite signs of the LOVP trends, blue and red combined to make purple. The valley and ridge stations are marked by circles and triangles, respectively. The Snotel stations are not included in the picture.

Table 4.2: The median, mean, standard deviation, maximum and minimum values of the LOVP trends for all three datasets. The numbers are in days/year and rounded to two decimal places. The negative numbers indicate a shortening of the LOVP, whereas the positive ones increasing LOVP trends.

	Median	**Mean**	**St. dev.**	**Maximum**	**Minimum**
Valley stations					
Raw	0.44	0.60	1.25	2.82	-0.65
Homogenized	-0.01	0.25	0.60	1.44	-0.14
Partially-homogenized	0.36	0.64	1.31	2.82	-1.06
Ridge stations					
Raw	0.00	-0.41	3.92	3.97	-18.71
Homogenized	-0.17	-0.81	3.74	3.89	-18.71
Partially-homogenized	0.04	-0.44	3.94	3.97	-18.71
All stations					
Raw	0.01	-0.24	3.61	3.97	-18.71
Homogenized	-0.03	-0.63	3.42	3.89	-18.71
Partially-homogenized	0.05	-0.26	3.64	3.97	-18.71

4.3 T_{min} and T_{max} trends

4.3.1 LSR PDF maxima

Here, only the T_{min} and T_{max} trends as assessed by the LSR PDF maxima are presented. For both of T_{min} and T_{max}, the majority of the stations exhibited a net warming trend for all three datasets. The choice of a dataset played a role. Fig. 4.4 shows the T_{min} and T_{max} trends for the HJA stations for all datasets, plotted on a topographic map of the HJA. The T_{min} and T_{max} trends are summarized in Tables 4.3 and 4.4, respectively.

For T_{min}, the valley stations showed a slightly more consistent warming signal than the ridge stations. For the raw and homogenized datasets, all of the valley stations showed a warming trend, with the exception of PRIMET450. The records for PRIMET150 spanned the period 1975-2011, whereas for PRIMET450 the span was only 1996-2011 and the standard deviations for PRIMET450 were also larger than for PRIMET150, as can be seen in Tables A.4 - A.6 in the Appendix. When the partially-homogenized dataset was used, the largest number of stations (25 out of 35, regarding the two heights of a benchmark stations as two stations) exhibited a warming trend, compared to the raw dataset (22 stations showed a warming trend) and the homogenized dataset (20 warming trends).

For T_{max}, the choice of the dataset played a considerable role. For the partially-homogenized dataset, all of the valley stations except PRIMET450 showed a warming trend, whereas in the case of the raw dataset, four out of six stations showed a cooling trend. Overall, when the partially-homogenized dataset was used, 25 out of the 35 stations showed a warming trend, compared to 19 and 18 warming trends in case of the homogenized and the raw dataset, respectively.

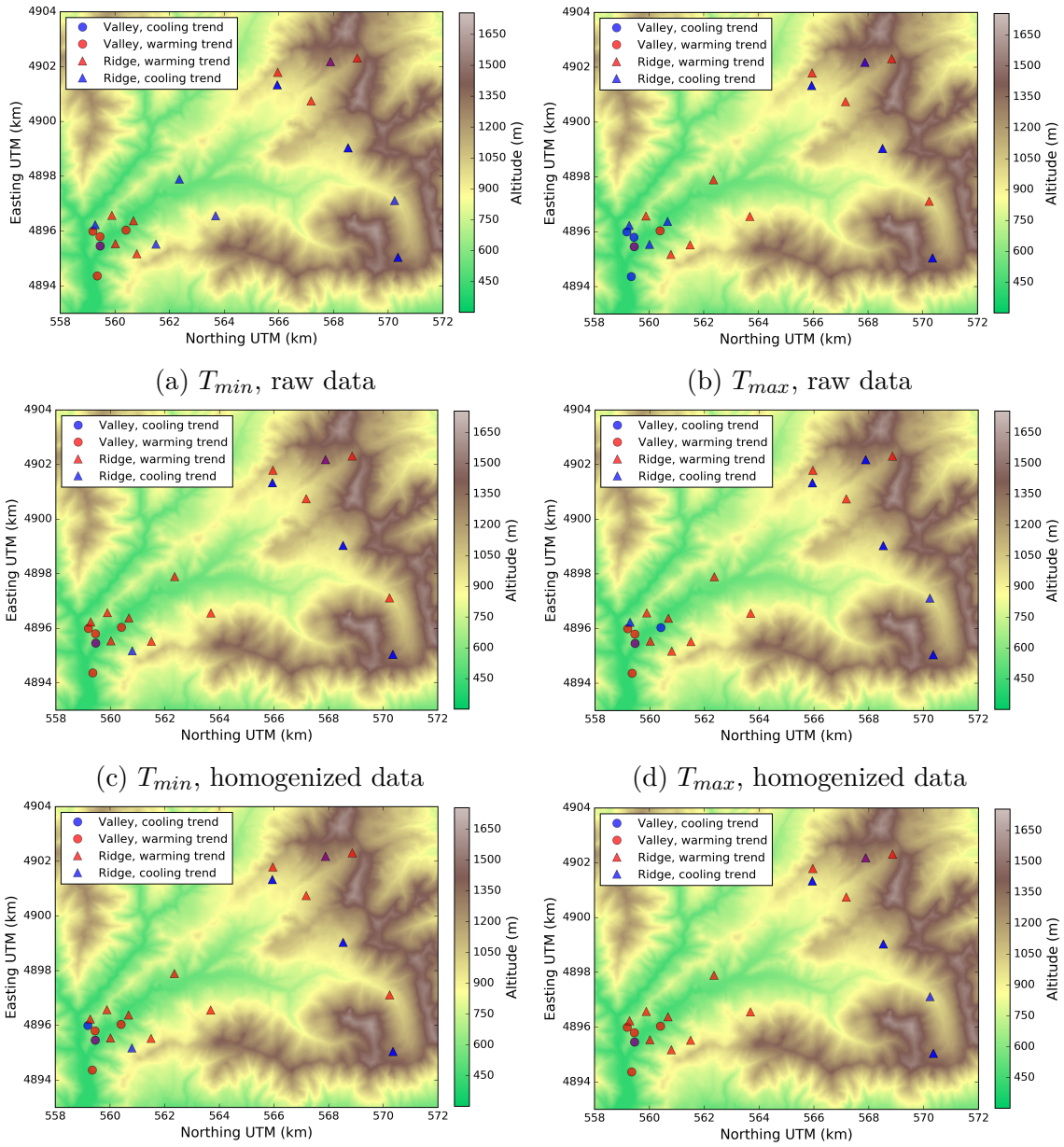

(a) T_{min}, raw data

(b) T_{max}, raw data

(c) T_{min}, homogenized data

(d) T_{max}, homogenized data

(e) T_{min}, partially-homogenized data

(f) T_{max}, partially-homogenized data

Figure 4.4: The T_{min} and T_{max} trends for the HJA stations, all datasets.

Table 4.3: The T_{min} trends minimum, mean, median and maximum values for all three datasets. The numbers are in K/decade and rounded to two decimal places. The negative numbers indicate cooling trends, whereas the positive ones warming T_{min} trends.

	Median	**Mean**	**St. dev.**	**Maximum**	**Minimum**
Valley stations					
Raw	0.13	0.16	0.38	0.72	-0.42
Homogenized	0.11	-0.01	0.38	0.24	-0.78
Partially-homogenized	0.20	0.15	0.36	0.63	-0.42
Ridge stations					
Raw	0.13	0.08	0.54	0.77	-1.19
Homogenized	0.01	-0.11	0.42	0.60	-1.11
Partially-homogenized	0.14	0.05	0.49	0.82	-1.19
All stations					
Raw	0.13	0.09	0.51	0.77	-1.19
Homogenized	0.04	-0.09	0.41	0.60	-1.11
Partially-homogenized	0.15	0.07	0.47	0.82	-1.19

Table 4.4: The T_{max} trends minimum, mean, median and maximum values for all three datasets. The numbers are in K/decade and rounded to two decimal places. The negative numbers indicate cooling trends, whereas the positive ones warming T_{max} trends.

	Median	**Mean**	**St. dev.**	**Maximum**	**Minimum**
Valley stations					
Raw	-0.03	-0.19	0.60	0.27	-1.36
Homogenized	0.12	-0.13	0.62	0.29	-1.36
Partially-homogenized	0.21	-0.04	0.66	0.39	-1.36
Ridge stations					
Raw	0.01	0.08	0.61	1.35	-0.92
Homogenized	0.02	-0.10	0.58	1.15	-1.95
Partially-homogenized	0.11	0.09	0.51	1.15	-0.92
All stations					
Raw	0.01	0.04	0.61	1.35	-1.36
Homogenized	0.03	-0.11	0.58	1.15	-1.95
Partially-homogenized	0.15	0.07	0.53	1.15	-1.36

4.3.2 Other parameters

Apart from the LSR PDF maxima, the Theil-Sen (TS) method was also used to analyze the trends in T_{min} and T_{max}. The maxima of PDF of DOY trends as well as means of DOY trends were considered for both the LSR and TS methods. An example result of the T_{min} and T_{max} trends at CS2MET for all three datasets can be seen in Fig. 4.5. There was a large variability among the DOY trends for both of the LSR and TS methods, with no clear seasonal patterns. The results for all stations and all datasets can be seen in Tables A.4 - A.6 in the Appendix.

For T_{min}, the valley stations showed a more consistent warming trend (considering the PDF maxima and means using the LSR and TS methods) than the ridge stations. For T_{max}, this was also true for the homogenized and partially-homogenized datasets, where at least four out of the six valley stations showed a warming trend. Similarly as in the case of the LSR PDF maxima, the TS method results were considerably affected by the choice of the dataset.

In the vast majority of cases, the standard deviations were larger than the absolute values of the corresponding trends, both for the LSR and TS methods, indicating a large spread of the trend values. There were differences between the results obtained by LSR and TS methods. Full results can be seen in Table A.4 in the Appendix.

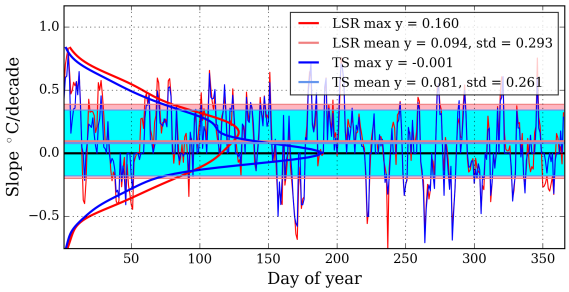

(a) T_{min}, raw data

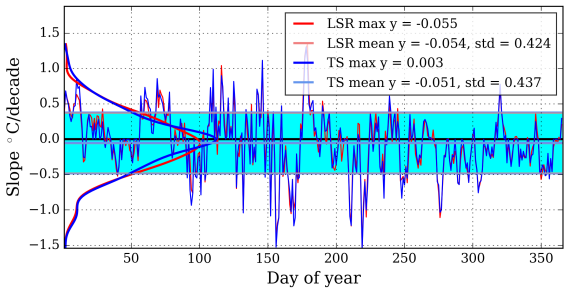

(b) T_{max}, raw data

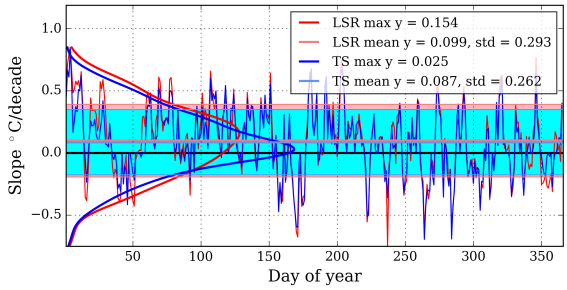

(c) T_{min}, homogenized data

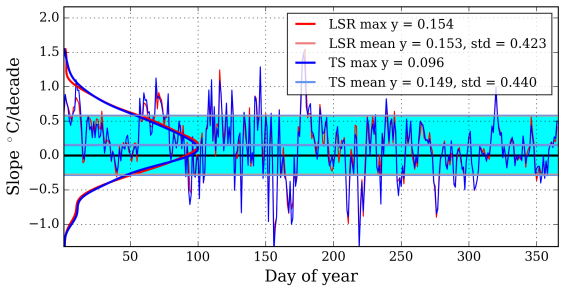

(d) T_{max}, homogenized data

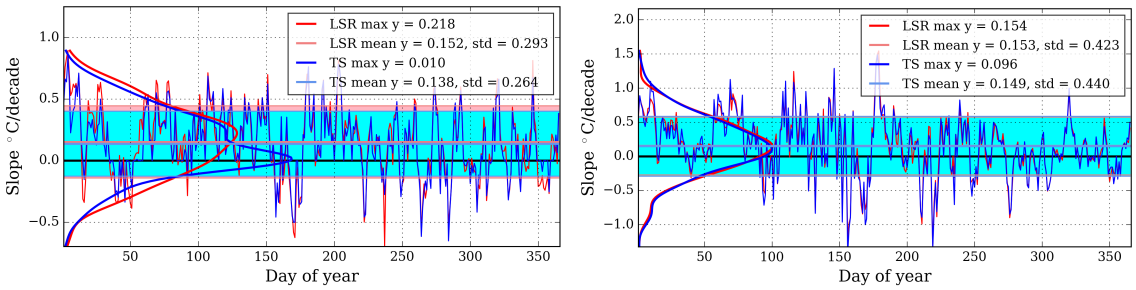

(e) T_{min}, partially-homogenized data (f) T_{max}, partially-homogenized data

Figure 4.5: The LSR (in red) and TS (blue) T_{min} and T_{max} trends at CS2MET for all three datasets. Various parameters were used: LSR PDF (red, approximately Gaussian curve); mean of DOY trends, LSR (pink vertical line); LS PDF (blue, approximately Gaussian curve); mean of DOY trends, TS (light blue vertical line). The pink and blue colored belts indicate the areas of ± one standard deviation from the LSR and TS methods means, respectively.

4.4 Synoptic patterns

As described in the section 3.8, for each year, the numbers of cyclonic, anti-cyclonic and zonal days were calculated. Three different variants were used for daily synoptic pattern classification: (a) $n_s \geq 3$ and $p_c \leq 0.05$, (b) $n_s \geq 2$ and $p_c \leq 0.1$ and (c) $n_s \geq 2$ and $p_c \leq 0.8$, where n_s is the number of data points (corresponding to stations) for a given date and p_c is the maximum accepted p-value. Fig. 4.6 shows Hovmöller diagrams for the cyclonic, anti-cyclonic and zonal days for the homogenized dataset. The results were similar for the raw and partially-homogenized dataset. There was a larger proportion of cyclonic days in the period March - May, compared to June - September.

Afterwards, for each year and each variant of conditions, the numbers of cyclonic, anti-cyclonic and zonal days obtained were multiplied by a constant such that they would add up to 365 days and trends in the annual number of days for each synoptic pattern were investigated. For the raw data, the annual numbers of cyclonic and zonal days exhibited positive trends and the annual number of anti-cyclonic days showed negative trends (Fig. 4.7). Likewise, in the case of the homogenized and partially-homogenized datasets, the annual number of anti-cyclonic days had negative trends, whereas the annual numbers of cyclonic and zonal days showed positive trends.

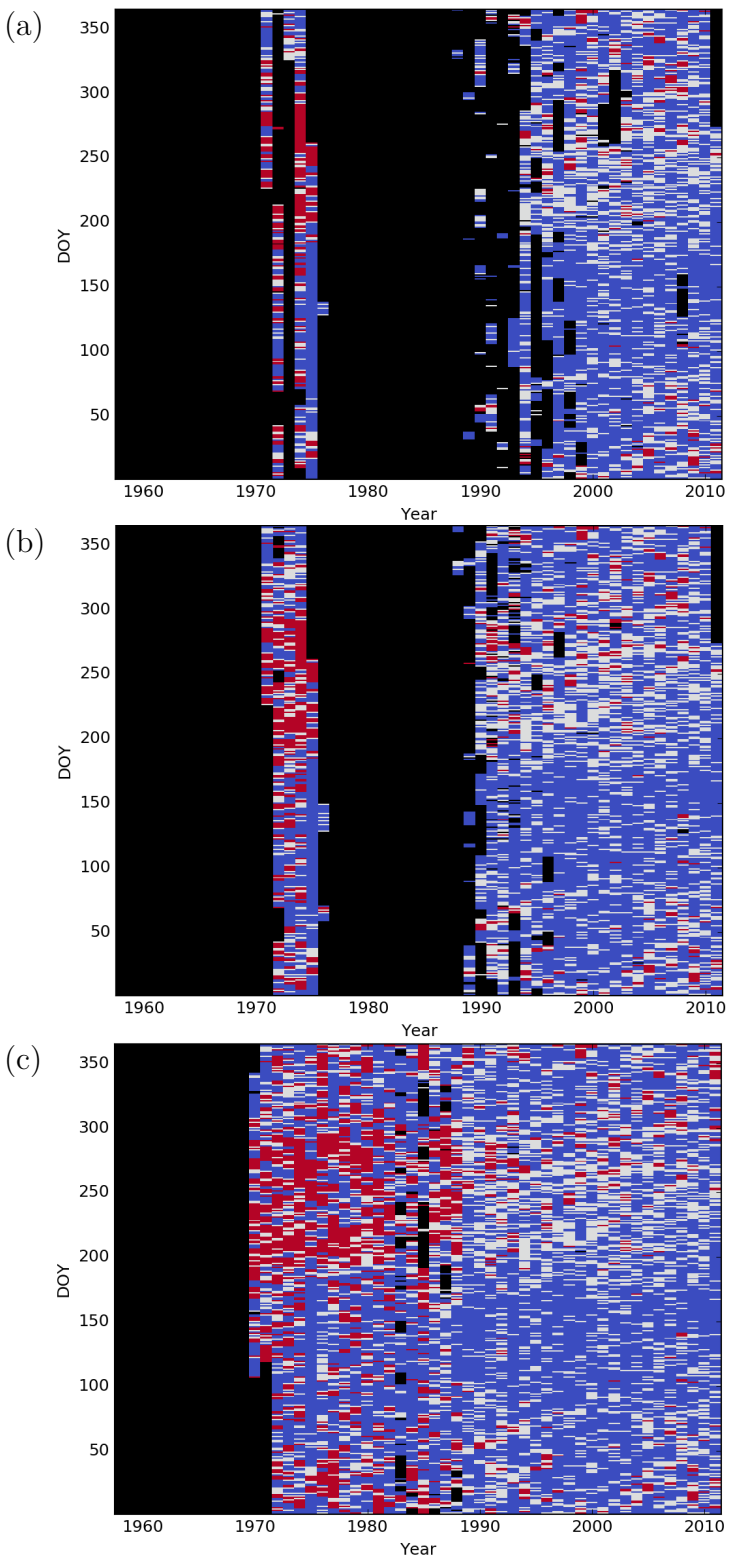

Figure 4.6: Synoptic patterns for the study area (the HJA and Snotel) showing cyclonic (blue), anti-cyclonic (red) and zonal days (grey) for homogenized data for (a) $n_s \geq 3$ and $p_c \leq 0.05$, (b) $n_s \geq 2$ and $p_c \leq 0.1$ and (c) $n_s \geq 2$ and $p_c \leq 0.8$. Black fields indicate no available data.

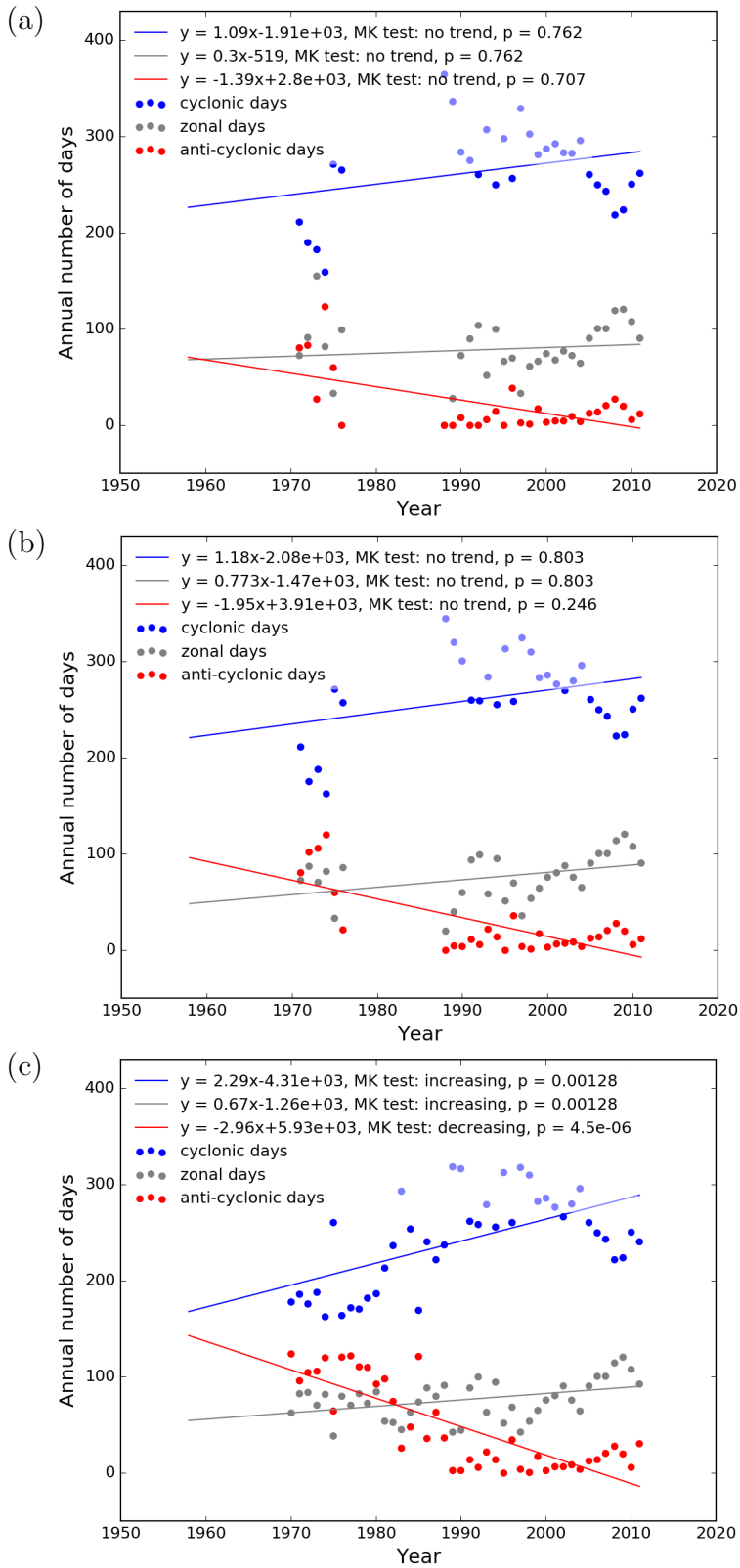

Figure 4.7: Trends of cyclonic (blue), anti-cyclonic (red) and zonal (grey) days over the study area (the HJA and Snotel) for the raw dataset and for (a) $n_s \geq 3$ and $p_c \leq 0.05$, (b) $n_s \geq 2$ and $p_c \leq 0.1$ and (c) $n_s \geq 2$ and $p_c \leq 0.8$.

4.5 Wind speed and direction

Wind speed and direction data were only available for the benchmark stations. A time series of mean night-time wind direction was plotted for all of the benchmark stations; Fig. 4.8 shows an example for PRIMET and Table 4.5 shows a summary for all of the benchmark stations.

Out of the benchmark stations available, PRIMET was the only valley station. When plotting the mean nigh-time wind direction at PRIMET, one can clearly see two main flows (Fig. 4.8), channeled along the valley. These were noted as the North-East (NE, here 0-90°) and South-West (SW, 180-270°) flows.

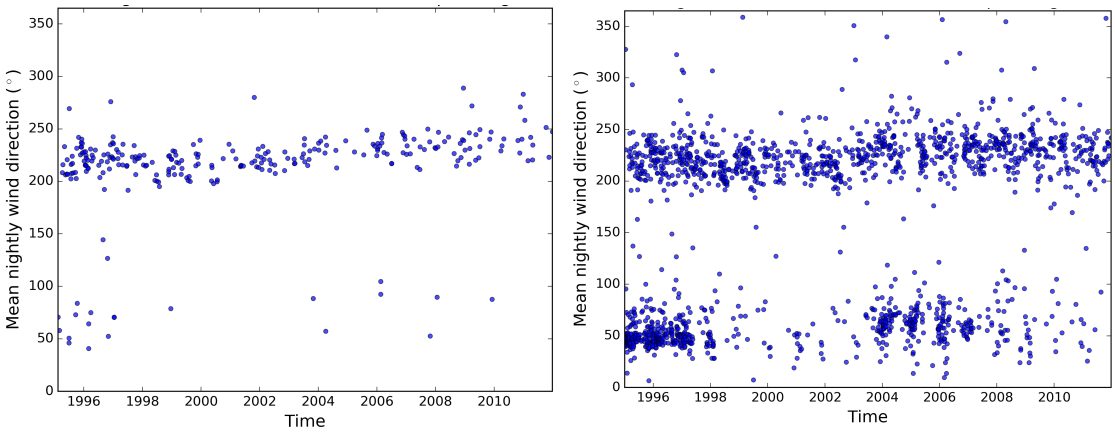

(a) Accepted flags: 'A'

(b) Accepted flags: 'A', 'B'

Figure 4.8: The mean nigh-time wind direction at PRIMET

Table 4.5: Mean night-time wind direction at benchmark stations.

Station	**Wind direction**
PRIMET	Two main flow directions can be seen: NE and SW, corresponding to up- and down-valley direction. Large proportion of the records have wind magnitudes < 1 m/s.
VANMET	Two main wind directions: around 200°(approximately SSW) and around 90°(E)
UPLMET	One main wind direction: around 210°(approximately SSW)
CENMET	One main wind direction: around 35°(approximately NE)
H15MET	A large proportion of the data has a wind magnitude < 1 m/s. Considering wind direction when flags 'A' and 'B' are accepted, there is a main flow at about 150°(approximately SSE), which weakened around 2005.

To investigate whether the nigh-time wind direction at PRIMET affects T_{min}, the mean night-time direction was plotted against T_{min} perturbation - here the difference

from the monthly mean (hence independent of the season). As Fig. 4.9 shows, the mean perturbation had higher value for the SW flow than for the NE flow, suggesting the days with prevailing NE flows had on average colder night temperatures than those with prevailing SW flows. The difference between SW mean T_{min} and NE mean T_{min} was especially pronounced when only the 'A' flags were accepted.

The values for the NE and SW mean and standard deviation were exactly the same for all three datasets. This was because only the differences from monthly temperature means were considered, hence shifting the temperature time series by a constant did not affect the results.

(a)

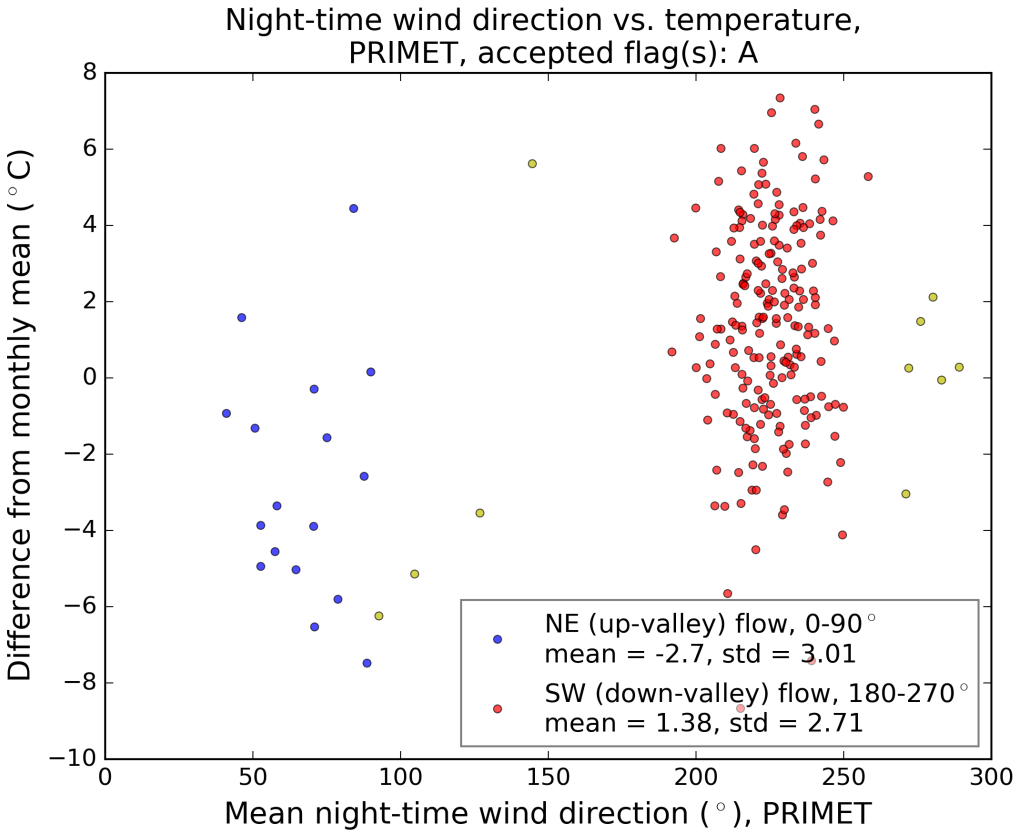

(b)

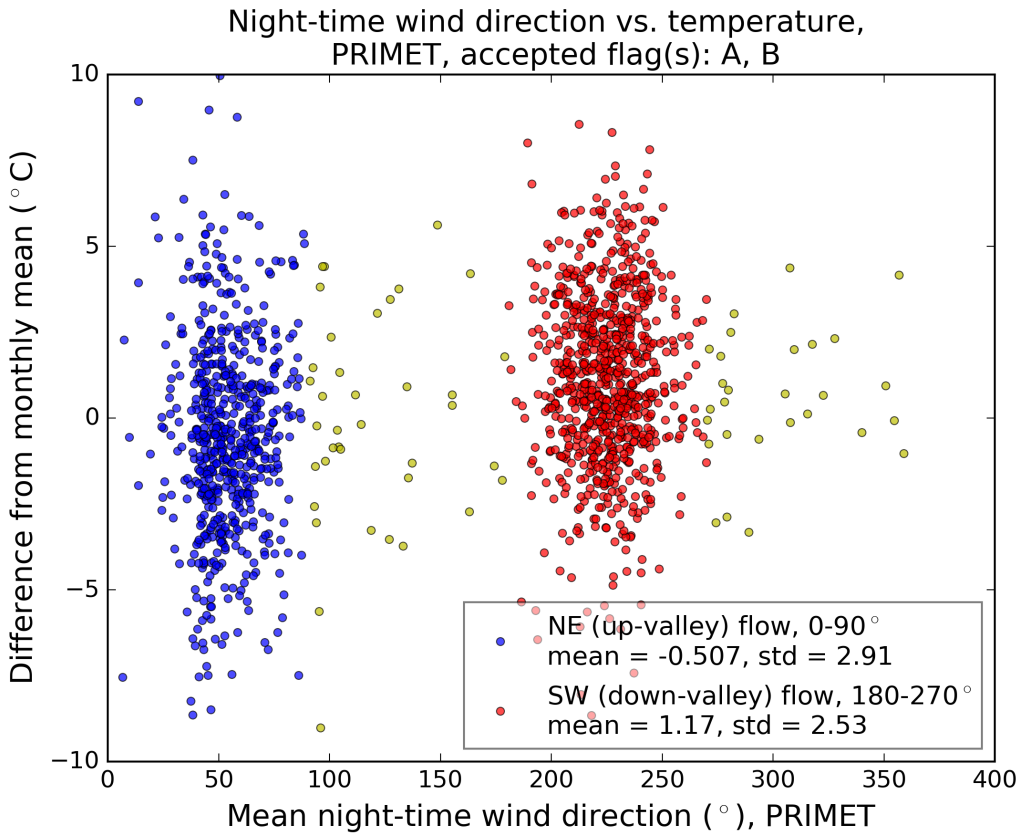

Figure 4.9: The difference from the monthly mean T_{min} (taken at height 4.5 m) as a function of mean night-time wind direction for PRIMET.

5 Discussion

5.1 Temperature patterns

The valley stations experienced a more pronounced LDOF trend compared to the ridge stations, contrary to the hypothesis. For most of the stations, an earlier LDOF was observed, in agreement with Kunkel *et al.* (2004) and results predicting increasing T_{min} trends (section 2.2.1).

There seems to be no distinct patterns in the LOVP for the valley and ridge stations, which does not support or undermine the hypothesis. Overall, it was found that the LOVP was increasing at the majority of the stations during the study period, in agreement with what was found by Kunkel *et al.* (2004). The records suffered from gaps that limited the analysis. In some cases, e.g. for UPLMET150, Fig. 4.2b, there were not enough data points to get a significant trend. At high elevations, frost can occur at any time of the year, therefore the LOVP is not meaningful there. A few of the stations studied, especially McKenzie, had a very short LOVP (Fig. 4.2c). Also, the differences in results for the two different heights (150 and 450 cm) for the benchmark stations seem to be relatively large (in some cases, the trends between the two heights at a benchmark station differed more than between one height and another station hundreds of meters away).

For both T_{min} and T_{max}, the majority of the stations exhibited a warming trend for all three datasets, which is in agreement with what was observed by others (section 2.2.1). For T_{min}, the valley stations showed a more consistent warming trend than the ridge stations, contrary to the hypothesis. However, in most cases, the p-values of the temperature trends considered were > 0.05. The resulting trends for the raw, homogenized and partially-homogenized datasets exhibited considerable differences, indicating that the presence of breaks in the raw time series affected the results, and this should not be neglected in future climate research. Good quality long-term datasets are highly valuable for climate change studies.

5.2 Synoptic patterns and wind

For all datasets, the annual number of anti-cyclonic days was decreasing, as indicated by the models considered in the IPCC AR4 2007. Anti-cyclonic flows with low flow

strength seem to lead to a more pronounced cold air pooling and hence stronger temperature inversions (Daly *et al.*, 2010). Therefore, the more pronounced warming trends of the valley stations could be explained by a decreasing number of anti-cyclonic days, which leads to less cold air pooling. This then causes a net warming at the valley stations. The ridge stations are likely less affected by the changing cold air pool patterns, as indicated by the results, especially for the LDOF and T_{min} trends. In future research, seasonal changes in the number of cyclonic, anti-cyclonic and zonal days could be considered.

At PRIMET, the only valley station with wind data, the mean night-time wind direction was largely channeled along the valley. It could be expected that during nights with a dominant cold air drainage and pooling, the wind direction was down-valley (SW), whereas during nights with dominant warm-air flows from the lake the direction was up-valley (NE). As Fig. 4.8 shows, a proportion of the nights had a mean night-time wind direction in between these two directions, indicating that the wind direction was likely changing during those nights.

Regarding the relationship between T_{min} and mean night-time direction, the days with prevailing NE flows had on average colder night temperatures than those with prevailing SW flows. The exact reason for this is unknown, however, one explanation could be that the area around PRIMET needs to be considerably colder than the lake for a SW flow of a detectable magnitude to be formed. Or, it could be due to the fact that flows with low strengths were not detected, which could introduce a considerable error in the mean night-time wind direction, especially for nights without any stronger flows. One could expect colder T_{min} for nights with prevalent cold air pooling, however, low flow strength is needed for a cold air pool to form, which might then go undetected by the wind monitors.

As Daly *et al.* (2010) found out, synoptic patterns affect formation of cold air pools, and anti-cyclonic patterns are most favorable for cold air drainage and pooling. However, as Fig. 4.7 shows, the anti-cyclonic days were in the minority compared to cyclonic and zonal days. Therefore, the overall mean of T_{min} perturbation (Fig. 4.9) was mostly affected by cyclonic and zonal days, with only shallow or absent cold air pools. Future research could address this by separating the anti-cyclonic, zonal and cyclonic days and calculating the mean T_{min} perturbation for each of these three synoptic patterns and the two identified wind directions at PRIMET. Also, wind monitors capable of detecting flows with lower strengths would be helpful in clarifying the observed temperature changes in the valley.

6 Conclusions

The hypothesis was not confirmed. In the case of the LDOF, the contrary seems more likely, as the valley stations experienced an earlier LDOF trend, whereas the ridge stations showed an inconsistent pattern. In the case of the LOVP, no distinct patterns were found. For T_{min}, the valley stations showed a more consistent warming trend than the ridge stations. For T_{max}, the same was true only for the partially-homogenized and homogenized dataset. The majority of the stations had temperature trends with p-values > 0.05.

Three datasets were used: raw, homogenized and partially-homogenized. The choice of dataset played a role in the results. In a number of cases, an observed trend a had smaller absolute magnitude than the change to its value when calculated using a different dataset. The effect of shifts and breaks in a time series should not be neglected in future climate research.

The annual numbers of cyclonic and zonal days showed increasing trends, whereas the annual number of anti-cyclonic days showed a decreasing trend. The exact mechanism is still debated, but changes in synoptic forcing towards more cyclonic activity and hence less cold air pooling in spring could serve as an explanation. In the HJA valley studied, two competing flows channeled along the valley were detected: NE down-valley flow and SW up-valley flow. Days with prevailing NE flows had on average colder night temperatures than those with prevailing SW flows. Further research and more data gathered over a longer period records are needed.

A Appendix

Table A.1: Stations' names (abbreviated and full) and geographical and topography information. The stations located less than 100 m above the valley bottom, i.e. below 530 asl, were marked as *valley* stations; all the other stations were marked as *ridge* stations. The geographical and topography information was provided by C. K. Thomas (2011).

Station name abbr.	Station name full	Latitude	Longitude	Northing UTM	Easting UTM	Elev. (m asl)	Aspect (°)	Slope (°)	Va./Ri.
PRIMET (150, 450)	Primary Meteorological Station	44.2119	-122.2558	4895461	559454.7	430	0	0	Valley
RS02	Reference Stand 2	44.217055	-122.2439	4896042.5	560400.9	480	285	22	Valley
CS2MET	Climatic Station at Watershed 2	44.215	-122.2492	4895805.5	559451.56	485	355	5	Valley
RS01	Reference Stand 1	44.202089	-122.2572	4894370	559349.4	499	200	41	Valley
RS89	Reference Stand 89	44.216742	-122.26	4895996	559188.3	514	315	37	Valley
RS17	Reference Stand 17	44.220111	-122.2404	4896384.5	560678.1	534	315	14	Ridge
RS07	Reference Stand 7	44.212599	-122.2488	4895544	560016.56	586	1	19	Ridge
RS86	Reference Stand 86	44.218849	-122.2579	4896231.5	559276.44	594	215	28	Ridge
RS10	Reference Stand 10	44.233571	-122.2191	4897895	562360.56	621	170	6	Ridge
RS24	Reference Stand 24	44.1711	-122.4236	4890821.5	546080.75	651	30	28	Ridge
RS20	Reference Stand 20	44.221909	-122.2503	4896577	559886.44	712	180	34	Ridge
RS16	Reference Stand 16	44.212326	-122.2402	4895527.5	561502.25	732	202	29	Ridge
RS15	Reference Stand 15	44.209253	-122.239	4895179	560800.8	755	350	33	Ridge
RS05	Reference Stand 5	44.221416	-122.2027	4896558	563684.25	907	10	12	Ridge
H15MET (150, 450)	High 15 Meteorological Station	44.2642	-122.1739	4901332.5	565939.44	922	240	15	Ridge
RS03	Reference Stand 3	44.258862	-122.1585	4900752	567177.5	978	315	5	Ridge
RS12	Reference Stand 12	44.22586	-122.1207	4897118.5	570233.9	987	282	11	Ridge
CENMET (150, 450)	Central Meteorological Station	44.2433	-122.1417	4899038	568533.6	1018	260	12	Ridge
RS26	Reference Stand 26	44.268287	-122.1736	4901787	565956.2	1054	180	20	Ridge
JumpOffJoe	Jump Off Joe	44.383	-122.167	4914751	566354	1073	NaN	NaN	Ridge
SantiamJunction	Santiam Junction	44.4333	-121.95	4920319.5	583570.5	1140	NaN	NaN	Ridge
VANMET (150, 450)	Vanilla Leaf Meteorological Station	44.2717	-122.1494	4902186	567886.25	1273	180	23	Ridge
UPLMET (150, 450)	Upper Lookout Meteorological Station	44.2072	-122.1194	4895046.5	570357.25	1294	72	13	Ridge
RS04	Reference Stand 4	44.272716	-122.1371	4902309	568864.8	1302	270	27	Ridge
RS13	Reference Stand 13	44.3439	-122.1233	4910227	569883.56	1350	270	20	Ridge
RS14	Reference Stand 14	44.327	-122.094	4908592	572238	1430	1	32	Ridge
McKenzie	McKenzie	44.2167	-121.8667	4896349.5	590532.8	1454	NaN	NaN	Ridge
HoggPass	Hogg Pass	44.4167	-121.85	4918582.5	591555.4	1460	NaN	NaN	Ridge
RoaringRiver	Roaring River	43.9	-122.028	4861086	584326.94	1509	NaN	NaN	Ridge
ThreeCreeksMeadow	Three Creeks Meadow	44.15	-121.6333	4889225	609300.94	1734	NaN	NaN	Ridge

Table A.2: The LDOF trends (in days/year) and their corresponding p-values for all stations and all three datasets. Trends corresponding to an earlier LDOF ('warming') are shown in red and p-values < 0.05 are in bold.

				Raw data		Homogenized data		Partially-homogenized data	
Station	**Elev. (m asl)**	**Aspect (°)**	**Slope (°)**	**LDOF trend (d/y)**	**p-value**	**LDOF trend (d/y)**	**p-value**	**LDOF trend (d/y)**	**p-value**
PRIMET450	430	0	0	-1.33	**0.010**	-0.40	0.835	-0.97	0.111
PRIMET150	430	0	0	-0.66	0.260	-0.04	0.914	-0.84	**0.000**
RS02	480	285	22	-0.53	0.334	-0.01	0.979	-0.08	0.695
CS2MET	485	355	5	-0.83	**0.043**	-0.28	0.057	-0.31	0.050
RS01	499	200	41	-0.72	**0.026**	-0.26	0.607	-0.46	0.381
RS89	514	315	37	-0.78	**0.014**	-0.02	0.960	0.70	0.074
RS17	534	315	14	-0.18	0.262	-0.65	0.448	-0.65	0.448
RS07	586	1	19	-0.97	0.111	-1.04	0.139	-1.04	0.139
RS86	594	215	28	-0.50	**0.021**	-0.14	0.563	-0.14	0.563
RS10	621	170	6	0.69	0.380	0.15	0.389	0.01	0.901
RS24	651	30	28	0.16	0.855	0.64	0.432	0.64	0.432
RS20	712	180	34	1.25	**0.047**	0.92	0.079	0.92	0.079
RS16	732	202	29	2.94	**0.019**	-0.32	0.791	-0.32	0.791
RS15	755	350	33	1.11	0.087	0.15	1.000	0.15	1.000
RS05	907	10	12	2.12	0.133	-0.01	0.987	-0.01	0.987
HI15MET450	922	240	15	-0.05	1.000	1.25	**0.047**	1.25	**0.047**
HI15MET150	922	240	15	1.51	0.133	2.94	**0.019**	2.94	**0.019**
RS03	978	315	5	-0.98	0.227	-0.27	0.956	-0.67	0.546
RS12	987	282	11	0.05	0.793	-0.07	0.434	-0.19	0.241
CENMET450	1018	260	12	-0.55	0.622	0.53	0.508	0.69	0.380
CENMET150	1018	260	12	-0.30	0.251	0.16	0.855	0.16	0.855
RS26	1054	180	20	0.24	0.551	0.58	0.058	0.58	0.058
JumpOffJoe	1073	NaN	NaN	-0.44	0.869	-1.03	0.134	-0.78	**0.014**
SaniamJunction	1140	NaN	NaN	0.48	0.102	-0.58	0.154	-0.83	**0.043**
VANMET450	1273	180	23	0.41	0.549	-0.05	1.000	-0.05	1.000
VANMET150	1273	180	23	-0.35	0.612	1.51	0.133	1.51	0.133
UPLMET450	1294	72	13	-0.05	0.514	1.11	0.087	1.11	0.087
UPLMET150	1294	72	13	-0.77	0.718	2.79	0.060	2.12	0.133
RS04	1302	270	27	0.96	0.649	-0.30	0.251	-0.30	0.251
RS13	1350	270	20	-0.51	1.000	-0.21	0.940	-0.21	0.940
RS14	1430	1	32	0.16	0.640	0.05	0.722	-0.05	0.418
McKenzie	1454	NaN	NaN	0.19	0.809	-0.11	0.833	-0.77	0.091
HoggPass	1460	NaN	NaN	-0.15	0.629	-0.01	0.955	-1.33	**0.010**
RoaringRiver	1509	NaN	NaN	0.17	0.905	-0.42	0.450	-0.53	0.334
ThreeCreeksM.	1734	NaN	NaN	0.28	0.297	0.06	1.000	-0.72	**0.026**

Table A.3: The LOVP trends (in days/year) and their corresponding p-values for all stations and all three datasets. Trends corresponding to an increasing LOVP ('warming') are shown in red and p-values < 0.05 are in bold.

				Raw data		Homogenized data		Partially-homogenized data	
Station	**Elev. (m asl)**	**Aspect (°)**	**Slope (°)**	**LOVP trend (d/y)**	**p-value**	**LOVP trend (d/y)**	**p-value**	**LOVP trend (d/y)**	**p-value**
PRIMET450	430	0	0	2.82	0.060	1.44	0.452	2.82	0.060
PRIMET150	430	0	0	0.67	0.332	-0.01	0.457	1.31	**0.003**
RS02	480	285	22	-0.41	0.233	-0.03	0.787	0.05	0.989
CS2MET	485	355	5	0.20	0.523	0.24	0.232	0.38	0.109
RS01	499	200	41	0.95	0.972	-0.01	0.897	0.35	0.745
RS89	514	315	37	-0.65	0.297	-0.14	0.800	-1.06	0.067
RS17	534	315	14	0.84	0.826	1.29	0.442	1.29	0.442
RS07	586	1	19	1.54	0.807	2.31	0.101	2.31	0.101
RS86	594	215	28	-0.74	0.284	-0.43	0.419	-0.43	0.419
RS10	621	170	6	-0.97	**0.043**	-0.15	0.680	0.05	0.957
RS24	651	30	28	-0.28	0.552	-1.31	0.112	-1.31	0.112
RS20	712	180	34	-0.39	0.333	-1.65	**0.012**	-1.65	**0.012**
RS16	732	202	29	-1.04	0.392	-0.28	0.913	-0.28	0.913
RS15	755	350	33	0.01	0.754	-1.22	1.000	-1.22	1.000
RS05	907	10	12	-0.19	0.498	0.04	0.843	0.04	0.843
HI15MET450	922	240	15	-2.55	0.088	-2.55	0.088	-2.55	0.088
HI15MET150	922	240	15	-3.67	0.764	-3.67	0.764	-3.67	0.764
RS03	978	315	5	2.18	0.184	0.94	0.436	1.48	0.213
RS12	987	282	11	-0.51	0.385	0.24	0.545	0.24	0.545
CENMET450	1018	260	12	-2.56	0.308	-2.13	0.462	-2.56	0.308
CENMET150	1018	260	12	3.89	0.221	3.89	0.221	3.89	0.221
RS26	1054	180	20	0.34	0.476	-0.74	0.159	-0.74	0.159
JumpOffJoe	1073	NaN	NaN	3.00	0.055	0.48	1.000	3.00	0.055
SaniamJunction	1140	NaN	NaN	1.68	**0.021**	1.14	0.093	1.68	**0.021**
VANMET450	1273	180	23	-0.63	0.452	-0.63	0.452	-0.63	0.452
VANMET150	1273	180	23	-18.71	0.296	-18.71	0.296	-18.71	0.296
UPLMET450	1294	72	13	-0.32	1.000	-0.32	1.000	-0.32	1.000
UPLMET150	1294	72	13	0.00	1.000	0.00	1.000	0.00	1.000
RS04	1302	270	27	0.10	0.799	0.10	0.799	0.10	0.799
RS13	1350	270	20	0.33	0.944	0.13	0.963	0.13	0.963
RS14	1430	1	32	-0.55	0.440	-0.66	0.416	-0.53	0.646
McKenzie	1454	NaN	NaN	0.96	0.424	-0.17	1.000	1.15	0.209
HoggPass	1460	NaN	NaN	3.97	**0.003**	0.54	0.656	3.97	**0.003**
RoaringRiver	1509	NaN	NaN	1.52	0.215	1.10	0.342	1.52	0.215
ThreeCreeksM.	1734	NaN	NaN	0.91	0.487	-1.19	**0.049**	0.91	0.487

Table A.4: Statistics of DOY trends, raw data. Positive ('warming') trends are shown in red.

				T_{min} trends (K/decade)						T_{max} trends (K/decade)					
Station	**Elev. (m asl)**	**Aspect (°)**	**Slope (°)**	**LSR max**	**LSR mean**	**LSR std**	**TS max**	**TS mean**	**TS std**	**LSR max**	**LSR mean**	**LSR std**	**TS max**	**TS mean**	**TS std**
PRIMET450	430	0	0	-0.418	-0.005	1.477	-0.335	-0.023	1.494	-1.361	-1.239	2.249	-1.491	-1.178	2.402
PRIMET150	430	0	0	0.376	0.442	0.477	0.376	0.418	0.455	0.265	0.319	0.722	0.265	0.278	0.751
RS02	480	285	22	0.022	0.131	0.398	0.070	0.114	0.374	0.239	0.445	0.681	0.282	0.426	0.707
CS2MET	485	355	5	0.160	0.094	0.293	-0.001	0.081	0.261	-0.055	-0.054	0.424	0.003	-0.051	0.437
RS01	499	200	41	0.719	0.755	0.958	0.824	0.729	0.927	-0.013	0.379	1.709	0.094	0.362	1.729
RS89	514	315	37	0.094	0.054	0.528	0.094	0.027	0.501	-0.227	-0.419	0.806	-0.227	-0.443	0.854
RS17	534	315	14	0.130	0.242	1.032	0.130	0.232	0.955	-0.461	-0.566	1.605	-0.672	-0.589	1.672
RS07	586	1	19	0.094	0.298	0.955	0.094	0.283	0.912	-0.330	0.133	1.459	-0.238	0.112	1.493
RS86	594	215	28	-0.051	-0.030	0.484	0.031	-0.037	0.471	-0.075	0.201	0.864	0.192	0.187	0.938
RS10	621	170	6	-0.175	-0.106	0.404	-0.201	-0.137	0.381	0.177	0.159	0.702	0.177	0.155	0.733
RS24	651	30	28	0.742	0.764	0.795	0.914	0.753	0.799	1.294	1.482	1.242	1.217	1.463	1.330
RS20	712	180	34	0.442	0.385	0.563	0.410	0.386	0.567	0.933	0.946	0.998	1.108	0.941	1.066
RS16	732	202	29	-0.020	0.296	1.256	0.113	0.252	1.212	0.797	-0.008	2.043	0.561	-0.037	2.104
RS15	755	350	33	0.623	0.795	1.427	0.537	0.714	1.352	0.012	0.112	2.061	0.270	0.103	2.095
RS05	907	10	12	-0.013	0.105	0.473	-0.128	0.050	0.478	0.339	0.293	0.741	0.244	0.283	0.784
HI15MET450	922	240	15	-0.674	-0.568	1.370	-0.763	-0.548	1.381	-0.711	-0.875	2.130	-0.574	-0.921	2.186
HI15MET150	922	240	15	-0.287	-0.104	1.628	-0.001	-0.093	1.617	-0.517	-0.714	2.263	-0.802	-0.678	2.463
RS03	978	315	5	0.775	0.922	1.500	0.868	0.885	1.465	0.690	1.024	2.137	0.450	0.951	2.214
RS12	987	282	11	-0.071	-0.087	0.418	-0.071	-0.090	0.382	0.177	0.422	0.747	0.228	0.408	0.775
CENMET450	1018	260	12	-1.185	-1.264	1.820	-0.967	-1.152	1.855	-0.133	-0.777	3.058	0.220	-0.709	3.186
CENMET150	1018	260	12	-1.045	-0.746	1.801	-1.163	-0.677	1.817	-0.375	-0.876	2.931	-0.709	-0.730	3.108
RS26	1054	180	20	0.643	0.384	0.683	0.156	0.396	0.674	0.612	0.684	0.998	0.612	0.660	1.056
JumpOffJoe	1073	NaN	NaN	0.443	0.336	0.960	0.012	0.293	0.796	-0.238	-0.184	1.516	-0.044	-0.170	1.506
SaniamJunction	1140	NaN	NaN	0.344	0.481	0.938	0.022	0.435	0.816	0.289	-0.123	1.325	0.069	-0.130	1.294
VANMET450	1273	180	23	0.140	-0.162	1.305	-0.076	-0.161	1.297	0.007	-0.161	1.874	0.112	-0.195	1.932
VANMET150	1273	180	23	-1.034	-0.839	2.552	-0.744	-0.882	2.622	-0.702	-1.316	4.161	-0.425	-1.077	4.433
UPLMET450	1294	72	13	-0.195	-0.416	1.726	-0.478	-0.398	1.778	-0.916	-0.899	2.666	-1.066	-0.843	2.734
UPLMET150	1294	72	13	-0.276	0.144	6.188	-0.736	0.015	6.880	-0.904	2.604	12.835	-0.904	2.577	13.030
RS04	1302	270	27	0.042	0.193	0.558	0.101	0.179	0.539	0.577	0.559	0.707	0.538	0.523	0.738
RS13	1350	270	20	0.580	0.701	0.745	0.580	0.687	0.745	1.351	1.341	0.971	1.181	1.283	1.013
RS14	1430	1	32	0.541	0.438	0.761	0.295	0.435	0.758	0.740	0.888	0.934	0.794	0.858	0.975
McKenzie	1454	NaN	NaN	0.376	0.103	1.882	-0.041	0.393	1.178	-0.334	-0.511	2.087	-0.042	-0.205	1.755
HoggPass	1460	NaN	NaN	0.746	0.743	0.983	0.001	0.664	0.902	0.234	-0.202	1.704	0.050	-0.295	1.683
RoaringRiver	1509	NaN	NaN	0.250	0.520	1.423	-0.010	0.509	1.167	0.074	-0.071	1.771	-0.018	-0.042	1.815
ThreeCreeksM.	1734	NaN	NaN	0.419	0.258	1.450	-0.033	0.285	1.260	-0.170	-0.173	1.577	0.033	-0.218	1.533
Number of stations with a warming trend				22	24		19	24		18	17		22	17	
Number of stations with a cooling trend				13	11		16	11		17	18		13	18	

Table A.5: Statistics of DOY trends, homogenized data. Positive ('warming') trends are shown in red.

				T_{min} trends (K/decade)						T_{max} trends (K/decade)					
Station	**Elev. (m asl)**	**Aspect (°)**	**Slope (°)**	**LSR max**	**LSR mean**	**LSR std**	**TS max**	**TS mean**	**TS std**	**LSR max**	**LSR mean**	**LSR std**	**TS max**	**TS mean**	**TS std**
PRIMET450	430	0	0	-0.781	-0.411	1.483	-0.781	-0.407	1.496	-1.361	-1.239	2.249	-1.491	-1.178	2.402
PRIMET150	430	0	0	0.106	0.168	0.474	0.079	0.152	0.452	0.091	0.150	0.722	0.091	0.108	0.754
RS02	480	285	22	0.122	0.205	0.400	0.146	0.187	0.375	-0.078	0.157	0.686	-0.035	0.131	0.717
CS2MET	485	355	5	0.154	0.099	0.293	0.025	0.087	0.262	0.154	0.153	0.423	0.096	0.149	0.440
RS01	499	200	41	0.235	0.290	0.953	0.235	0.262	0.916	0.140	0.503	1.705	0.248	0.472	1.725
RS89	514	315	37	0.078	0.057	0.531	0.078	0.032	0.504	0.286	0.093	0.808	0.286	0.079	0.863
RS17	534	315	14	0.059	0.157	1.031	0.118	0.138	0.956	0.256	0.174	1.600	0.046	0.158	1.666
RS07	586	1	19	0.234	0.391	0.964	0.295	0.376	0.900	0.021	0.453	1.472	0.114	0.440	1.521
RS86	594	215	28	0.097	0.115	0.487	0.070	0.106	0.467	-0.129	0.030	0.857	0.029	0.012	0.936
RS10	621	170	6	0.113	0.176	0.402	0.036	0.144	0.373	0.206	0.223	0.703	0.206	0.219	0.739
RS24	651	30	28	0.265	0.268	0.793	0.322	0.257	0.786	0.472	0.675	1.231	0.242	0.662	1.320
RS20	712	180	34	0.145	0.080	0.577	0.082	0.076	0.570	0.034	0.051	0.989	0.034	0.032	1.052
RS16	732	202	29	0.044	0.315	1.256	0.247	0.264	1.208	1.146	0.457	2.046	0.910	0.417	2.102
RS15	755	350	33	-0.044	0.002	1.440	-0.216	-0.030	1.351	0.062	0.214	2.075	0.192	0.232	2.107
RS05	907	10	12	0.125	0.210	0.467	-0.046	0.156	0.472	0.296	0.281	0.738	0.248	0.267	0.780
HI15MET450	922	240	15	-0.556	-0.410	1.376	-0.556	-0.413	1.380	-0.711	-0.875	2.130	-0.574	-0.921	2.186
HI15MET150	922	240	15	-0.287	-0.104	1.628	-0.001	-0.093	1.617	-0.517	-0.714	2.263	-0.802	-0.678	2.463
RS03	978	315	5	0.598	0.618	1.498	0.785	0.572	1.451	0.139	0.356	2.123	-0.104	0.286	2.179
RS12	987	282	11	0.012	0.010	0.421	-0.014	0.004	0.385	-0.146	0.043	0.744	-0.095	0.023	0.770
CENMET450	1018	260	12	-0.644	-0.669	1.819	-0.427	-0.567	1.846	-0.919	-1.536	3.060	-0.565	-1.450	3.156
CENMET150	1018	260	12	-1.045	-0.746	1.801	-1.163	-0.677	1.817	-0.375	-0.876	2.931	-0.709	-0.730	3.108
RS26	1054	180	20	0.224	-0.026	0.698	-0.385	-0.023	0.680	0.114	0.147	1.012	0.114	0.129	1.053
JumpOffJoe	1073	NaN	NaN	-0.014	-0.008	0.968	-0.014	-0.042	0.790	-0.026	0.024	1.519	-0.026	0.031	1.502
SaniamJunction	1140	NaN	NaN	-0.080	0.061	0.935	-0.015	0.032	0.783	0.349	-0.069	1.319	0.056	-0.098	1.309
VANMET450	1273	180	23	0.140	-0.162	1.305	-0.076	-0.161	1.297	-0.181	-0.439	1.880	-0.288	-0.481	1.939
VANMET150	1273	180	23	-1.034	-0.839	2.552	-0.744	-0.882	2.622	-0.702	-1.316	4.161	-0.425	-1.077	4.433
UPLMET450	1294	72	13	-0.195	-0.416	1.726	-0.478	-0.398	1.778	-0.916	-0.899	2.666	-1.066	-0.843	2.734
UPLMET150	1294	72	13	-1.112	-1.853	6.149	-2.033	-1.891	6.686	-1.946	0.523	12.443	-1.946	0.516	12.855
RS04	1302	270	27	0.042	0.193	0.558	0.101	0.179	0.539	0.211	0.165	0.710	0.172	0.129	0.734
RS13	1350	270	20	0.140	0.247	0.740	0.140	0.236	0.730	0.681	0.633	0.970	0.396	0.575	1.005
RS14	1430	1	32	0.299	0.194	0.758	0.055	0.192	0.752	0.239	0.362	0.933	0.293	0.338	0.974
McKenzie	1454	NaN	NaN	-0.069	-0.114	1.789	-0.069	0.030	1.248	-0.278	-0.467	1.755	-0.056	-0.466	1.761
HoggPass	1460	NaN	NaN	-0.189	-0.221	1.000	0.003	-0.228	0.884	0.234	-0.202	1.704	0.050	-0.295	1.683
RoaringRiver	1509	NaN	NaN	-0.454	-0.169	1.423	-0.062	-0.082	1.148	-0.101	-0.259	1.780	-0.008	-0.250	1.843
ThreeCreeksM.	1734	NaN	NaN	-0.048	-0.203	1.449	-0.048	-0.149	1.239	-0.457	-0.415	1.581	0.049	-0.490	1.568
Number of stations with a warming trend				20	20		17	20		19	22		20	22	
Number of stations with a cooling trend				15	15		18	15		16	13		15	13	

Table A.6: Statistics of DOY trends, partially-homogenized data. Positive ('warming') trends are shown in red.

				T_{min} trends (K/decade)						T_{max} trends (K/decade)					
Station	**Elev. (m asl)**	**Aspect (°)**	**Slope (°)**	**LSR max**	**LSR mean**	**LSR std**	**TS max**	**TS mean**	**TS std**	**LSR max**	**LSR mean**	**LSR std**	**TS max**	**TS mean**	**TS std**
PRIMET450	430	0	0	-0.418	-0.005	1.477	-0.335	-0.023	1.494	-1.361	-1.239	2.249	-1.491	-1.178	2.402
PRIMET150	430	0	0	0.628	0.692	0.477	0.656	0.669	0.458	0.265	0.319	0.722	0.265	0.278	0.751
RS02	480	285	22	0.177	0.258	0.402	0.225	0.238	0.379	0.063	0.301	0.685	0.106	0.275	0.716
CS2MET	485	355	5	0.218	0.152	0.293	0.010	0.138	0.264	0.154	0.153	0.423	0.096	0.149	0.440
RS01	499	200	41	0.367	0.433	0.960	0.420	0.402	0.923	0.265	0.664	1.711	0.481	0.639	1.721
RS89	514	315	37	-0.075	-0.062	0.532	-0.046	-0.086	0.506	0.394	0.187	0.809	0.485	0.168	0.865
RS17	534	315	14	0.059	0.157	1.031	0.118	0.138	0.956	0.256	0.174	1.600	0.046	0.158	1.666
RS07	586	1	19	0.234	0.391	0.964	0.295	0.376	0.900	0.221	0.647	1.466	0.313	0.639	1.513
RS86	594	215	28	0.097	0.115	0.487	0.070	0.106	0.467	0.093	0.310	0.857	0.305	0.288	0.934
RS10	621	170	6	0.181	0.266	0.399	0.130	0.228	0.374	0.706	0.697	0.702	0.706	0.690	0.736
RS24	651	30	28	0.265	0.268	0.793	0.322	0.257	0.786	0.472	0.675	1.231	0.242	0.662	1.320
RS20	712	180	34	0.145	0.080	0.577	0.082	0.076	0.570	0.266	0.271	0.992	0.266	0.247	1.052
RS16	732	202	29	0.044	0.315	1.256	0.247	0.264	1.208	1.146	0.457	2.046	0.910	0.417	2.102
RS15	755	350	33	-0.044	0.002	1.440	-0.216	-0.030	1.351	0.062	0.214	2.075	0.192	0.232	2.107
RS05	907	10	12	0.125	0.210	0.467	-0.046	0.156	0.472	0.770	0.754	0.740	0.675	0.730	0.791
HI15MET450	922	240	15	-0.556	-0.410	1.376	-0.556	-0.413	1.380	-0.711	-0.875	2.130	-0.574	-0.921	2.186
HI15MET150	922	240	15	-0.287	-0.104	1.628	-0.001	-0.093	1.617	-0.517	-0.714	2.263	-0.802	-0.678	2.463
RS03	978	315	5	0.816	0.908	1.509	0.910	0.843	1.448	0.410	0.719	2.129	0.169	0.647	2.199
RS12	987	282	11	0.070	0.081	0.422	0.018	0.073	0.383	-0.146	0.043	0.744	-0.095	0.023	0.770
CENMET450	1018	260	12	-1.185	-1.264	1.820	-0.967	-1.152	1.855	-0.133	-0.777	3.058	0.220	-0.709	3.186
CENMET150	1018	260	12	-1.045	-0.746	1.801	-1.163	-0.677	1.817	-0.375	-0.876	2.931	-0.709	-0.730	3.108
RS26	1054	180	20	0.224	-0.026	0.698	-0.385	-0.023	0.680	0.114	0.147	1.012	0.114	0.129	1.053
JumpOffJoe	1073	NaN	NaN	0.443	0.336	0.960	0.012	0.293	0.796	-0.238	-0.184	1.516	-0.044	-0.170	1.506
SaniamJunction	1140	NaN	NaN	0.344	0.481	0.938	0.022	0.435	0.816	0.503	0.145	1.323	-0.009	0.126	1.297
VANMET450	1273	180	23	0.140	-0.162	1.305	-0.076	-0.161	1.297	0.007	-0.161	1.874	0.112	-0.195	1.932
VANMET150	1273	180	23	-1.034	-0.839	2.552	-0.744	-0.882	2.622	-0.702	-1.316	4.161	-0.425	-1.077	4.433
UPLMET450	1294	72	13	-0.195	-0.416	1.726	-0.478	-0.398	1.778	-0.916	-0.899	2.666	-1.066	-0.843	2.734
UPLMET150	1294	72	13	-0.276	0.144	6.188	-0.736	0.015	6.880	-0.904	2.604	12.835	-0.904	2.577	13.030
RS04	1302	270	27	0.042	0.193	0.558	0.101	0.179	0.539	0.211	0.165	0.710	0.172	0.129	0.734
RS13	1350	270	20	0.224	0.333	0.742	0.273	0.318	0.739	0.681	0.633	0.970	0.396	0.575	1.005
RS14	1430	1	32	0.529	0.421	0.762	0.284	0.416	0.747	0.501	0.638	0.935	0.501	0.605	0.964
McKenzie	1454	NaN	NaN	0.654	0.362	1.884	0.097	0.670	1.191	0.020	-0.290	2.089	-0.126	-0.007	1.777
HoggPass	1460	NaN	NaN	0.746	0.743	0.983	0.001	0.664	0.902	0.234	-0.202	1.704	0.050	-0.295	1.683
RoaringRiver	1509	NaN	NaN	0.250	0.520	1.423	-0.010	0.509	1.167	0.456	0.305	1.779	0.084	0.318	1.814
ThreeCreeksM.	1734	NaN	NaN	0.419	0.258	1.450	-0.033	0.285	1.260	0.071	0.099	1.579	-0.031	0.036	1.551
Number of stations with a warming trend				25	25		20	24		25	24		23	24	
Number of stations with a cooling trend				10	10		15	11		10	11		12	11	

Bibliography

Aguado, Edward 2016 *Understanding weather and climate, pp. 89-90*. Pearson.

Alexandersson, Hans 1986 A homogeneity test applied to precipitation data. *Journal of climatology* **6** (6), 661–675.

Alexandersson, Hans & Moberg, Anders 1997 Homogenization of Swedish temperature data. Part I: Homogeneity test for linear trends. *International Journal of climatology* **17** (1), 25–34.

Barry, Roger G & Blanken, Peter D 2016 *Microclimate and Local Climate, chapter 8 D*. Cambridge University Press.

Beniston, Martin 2006 Mountain weather and climate: a general overview and a focus on climatic change in the Alps. *Hydrobiologia* **562** (1), 3–16.

Bootsma, A 1976 Estimating minimum temperature and climatological freeze risk in hilly terrain. *Agricultural Meteorology* **16** (3), 425–443.

Brachet, Pascal 2014 Texmaker 4.4.1. URL `http://www.xm1math.net/texmaker/` – Accessed: 25.07.2017.

Daly, Christopher, Conklin, David R & Unsworth, Michael H 2010 Local atmospheric decoupling in complex topography alters climate change impacts. *International Journal of Climatology* **30** (12), 1857–1864.

Easterling, David R 2002 Recent changes in frost days and the frost-free season in the United States. *Bulletin of the American Meteorological Society* **83** (9), 1327–1332.

Foken, Thomas & Nappo, Carmen J 2008 *Micrometeorology*. Springer.

Geiger, Rudolf, Aron, Robert H & Todhunter, Paul 1995 *The climate near the ground, chapter 7*.

GLITCH 2016 3.0 beta release of the national water and climate center's interactive map. URL `http://andlter.forestry.oregonstate.edu/data/register/getdata.aspx?requestor_id=1930&entnum=14&dbcode=MS001&datapage=page2_static_ascii` – Accessed: 24.06.2017.

Greenland, David 1994 Regional context of the climate of HJ Andrews experimental forest, Oregon .

HJA Website 2017*a* HJ Andrews experimental forest. URL `https://andrewsforest.oregonstate.edu/` – Accessed: 12.06.2017.

HJA Website 2017*b* HJ Andrews experimental forest meteorological measurements information. URL `http://andlter.forestry.oregonstate.edu/Data/meta.aspx` – Accessed: 12.06.2017.

Holden, Zachary A, Abatzoglou, John T, Luce, Charles H & Baggett, L Scott 2011 Empirical downscaling of daily minimum air temperature at very fine resolutions in complex terrain. *Agricultural and Forest Meteorology* **151** (8), 1066–1073.

Jones, Julia 2010 Climate change effects on physical and biological systems in and near the Andrews Forest, Oregon. Presentation. URL `http://studylib.net/doc/12580234/climate-change-effects-on-physical-and-andrews-forest--or...` – Accessed: 26.7.2017.

Jones, PD, Trenberth, KE, Ambenje, P, Bojariu, R, Easterling, D, Klein, T, Parker, D, Renwick, J, Rusticucci, M, Soden, B *et al.* 2007 IPCC AR4, observations: surface and atmospheric climate change. pp. 235–336.

Kunkel, Kenneth E, Easterling, David R, Hubbard, Kenneth & Redmond, Kelly 2004 Temporal variations in frost-free season in the united states: 1895–2000. *Geophysical Research Letters* **31** (3).

Lundquist, Jessica D, Pepin, Nicholas & Rochford, Caitlin 2008 Automated algorithm for mapping regions of cold-air pooling in complex terrain. *Journal of Geophysical Research: Atmospheres* **113** (D22).

Mahrt, L, Richardson, Scott, Seaman, Nelson & Stauffer, David 2010 Non-stationary drainage flows and motions in the cold pool. *Tellus A* **62** (5), 698–705.

Marvin, Charles Frederick 1914 Air drainage explained. *Monthly Weather Review* **42** (10), 583–585.

Peterson, Thomas C & Easterling, David R 1994 Creation of homogeneous composite climatological reference series. *International journal of climatology* **14** (6), 671–679.

Pierre Raybaut and the Spyder Development Team 2017 Spyder 2.3.8, the scientific python development environment. URL `https://github.com/spyder-ide/spyder` – Accessed: 24.06.2017.

Python Software Foundation 2017 Python programming language, version 2.7. URL `http://www.python.org` – Accessed: 24.06.2017.

Smith, Jonathan W 2002 *Mapping the thermal climate of the HJ Andrews Experimental Forest, Oregon*. Master's thesis, Oregon State University.

Stocker, Thomas F, Qin, Dahe, Plattner, G-K, Alexander, Lisa V, Allen, Simon K, Bindoff, Nathaniel L, Bréon, F-M, Church, John A, Cubasch, Ulrich, Emori, Seita *et al.* 2013 IPCC AR5, technical summary, climate change 2013: The physical science basis. contribution of working group i to the fifth assessment report of the intergovernmental panel on climate change. pp. 33–115. Cambridge University Press.

Thanh, Han The 2015 pdftex 3.14159265-2.6-1.40.16 (tex live 2015/debian). URL `http://www.tug.org/applications/pdftex/` – Accessed: 25.07.2017.

The MathWorks, Inc. 2017 Matlab, version r2014b. URL `https://www.mathworks.com/` – Accessed: 25.7.2017.

USDA NRCS 2016*a* 3.0 beta release of the national water and climate center's interactive map. URL `https://www.wcc.nrcs.usda.gov/snow/snow_map_beta.html` – Accessed: 12.06.2017.

USDA NRCS 2016*b* Snow telemetry (Snotel) and snow course data and products. URL `https://www.wcc.nrcs.usda.gov/snow/snow_map_beta.html` – Accessed: 12.06.2017.

USDA NRCS 2017 Snotel, current or historic data. URL `https://wcc.sc.egov.usda.gov/nwcc/temptable` – Accessed: 25.7.2017.

Vose, Russell S, Easterling, David R & Gleason, Byron 2005 Maximum and minimum temperature trends for the globe: An update through 2004. *Geophysical Research Letters* **32** (23).

Whiteman, C David 2000 *Mountain meteorology: fundamentals and applications*. Oxford University Press.

Yue, Sheng, Pilon, Paul & Cavadias, George 2002 Power of the Mann–Kendall and Spearman's rho tests for detecting monotonic trends in hydrological series. *Journal of hydrology* **259** (1), 254–271.